Thermodynamic study of single crystal, Ni-based superalloys in the γ+γ' two-phase region using Knudsen effusion mass spectrometry, DSC and SEM

Spathara, Dimitra; Sergeev, Dmitry; Kobertz, Dietmar; Michael Müller, Michael; Putman, Duncan; Warnken, Nils

DOI:
10.1016/j.jallcom.2021.159295

Document Version
Peer reviewed version

Citation for published version (Harvard):
Spathara, D, Sergeev, D, Kobertz, D, Michael Müller, M, Putman, D & Warnken, N 2021, 'Thermodynamic study of single crystal, Ni-based superalloys in the γ+γ' two-phase region using Knudsen effusion mass spectrometry, DSC and SEM', *Journal of Alloys and Compounds*, vol. 870, 159295.
https://doi.org/10.1016/j.jallcom.2021.159295

Thermodynamic Study of Single Crystal, Ni-based Superalloys at the γ+γ' Two-phase Region Using Knudsen Effusion Mass Spectrometry, DSC and SEM.

Dimitra Spathara[a], Dmitry Sergeev[b], Dietmar Kobertz[b], Michael Müller[b], Duncan Putman[c], Nils Warnken[a]

[a] University of Birmingham, School of Metallurgy and Materials, Edgbaston, Birmingham B15 2TT, United Kingdom

[b] Forschungszentrum Jülich GmbH, Institute of Energy and Climate Research (IEK-2), 52425 Jülich, Germany

[c] Rolls-Royce plc, Derby DE24 8BJ, United Kingdom

Corresponding Author: Dimitra Spathara, University of Birmingham, School of Metallurgy and Materials, Edgbaston, Birmingham B15 2TT, United Kingdom d.spathara@bham.ac.uk

Keywords: activity, sublimation, vaporisation, Knudsen effusion mass spectrometry, high-temperature alloys, gas-solid reactions

Abstract

Second and third generation single crystal (SX) Ni-based superalloys are considered to be sensitive to microsegragation, incipient melting and microstructural instability. Thus, their thermodynamic properties and stability at high temperatures are of key importance. Vapour composition consisting of four species has been detected in the temperature range 1453-1573 K. This was found after studies of three single crystal Ni-based superalloys CMSX-4, CMSX-10K and CMSX-10N using the method of Knudsen Effusion Mass Spectrometry (KEMS). The activities of Ni, Co, Cr, and Al have been determined in the γ+γ', two-phase region. A series of Differential Scanning Calorimetry (DSC) measurements were carried out at various ramping up rates to determine phase transition temperatures; the γ' solvus, the solidus and the liquidus temperature were obtained. Back-scattered Electron Imaging (BEI) and Energy Dispersive Spectroscopy (EDS) measurements were performed and depicted the effect post KEMS for such complex multicomponent systems.

Introduction

Ni-based superalloys are among the most complex alloys that have found widespread technical applications [1-4]. Single crystal superalloys commonly consist of nine to ten major alloying elements, plus several minor elements and controlled content of impurities. Manufacturing involves directional solidification with investment casting exhibiting microsegregation phenomena, which leads to the formation of γ dendrites and interdendritic γ′, where γ is the fcc disordered, Ni-solid solution phase and γ’ (L12), is a Ni_3Al phase with solubility for some alloying elements such as Ta, Ti and others [4, 5]. The solidification path during casting deviates significantly from the equilibrium solidification path, which makes a subsequent solution heat treatment necessary [6].

The in-service microstructure, for which these alloys are designed, on the other hand is surprisingly simple, consisting of only two phases. Precipitates of the ordered γ' phase (L12 structure) are embedded in a disordered matrix of γ phase (fcc structure). Single crystal alloys are commonly designed to maximise the content of strengthening alloying elements. However, they are prone to microstructural instability, with detrimental impact to their mechanical properties, which commonly results in the formation of Topologically Closed Packed phases (TCP) [7-9]. They form due to the presence of large amounts of elements such as W and Re [10]. Elements like Cr, Co and Mo also promote TCP formation [2-6]. Thus, in order to achieve the optimum microstructure, the content of alloying elements needs to be carefully balanced, while maintaining mechanical properties, oxidation resistance, and manufacturability among other properties. This makes tasks such as alloy development or rationalising changes in the alloy during processing and service formidable, which cannot be mastered by intuition alone [11]. Current thermodynamic models of alloy constitution, utilising the CALPHAD method, are an essential tool in the metallurgist’s toolbox. The CALPHAD method uses models for the Gibbs free energy (Gibbs energy for short) to describe alloy thermodynamics and provide useful insight such as phase diagrams [4, 5]. In order to describe Gibbs energies, experimental data is required. The most widely available data is of course phase diagram data, microstructures for given alloy composition-temperature combinations and some transition temperatures, such as liquidus temperature, which can be easily obtained from DSC measurements. These datasets allow modelling the thermodynamics of an alloy system and calculate phase diagrams. It has been demonstrated however that two completely different sets of thermodynamic descriptions can produce equally accurate reproductions of a phase diagram [12], as phase equilibrium data does not give any hint on the underlying thermodynamic properties of the system. This rather unsatisfying situation can be remedied by including measured thermodynamic properties into the assessment. Measuring thermodynamic properties however requires significantly more

effort and specialised equipment and is thus less commonly undertaken. Thermodynamic properties, such as activities or heat capacities, are therefore less frequently studied than data on alloy constitution, although this would provide deeper insight into the thermodynamics of alloys. This becomes especially problematic when these quantities are later obtained from CALPHAD data, which has been modelled based on phase equilibrium data only, and then used for modelling of for example microstructure evolution during processing and service, as for instance during oxidation [13]. This can result in correct reproduction of phase equilibria, but wrong thermodynamic data, such as activities or heat capacities.

The present paper is aiming to address this lack of thermodynamic data by presenting a study on the activities of some alloying elements in three very common Ni-based single crystal superalloys. Activities were measured using the well-established method of Knudsen Effusion Mass Spectrometry (KEMS) [14-21]. Hilpert et al. [22, 23] studied the Ni-Al phase diagram using KEMS at the Ni-rich area of >0.7at% and Copland [24] proposed an updated version of the Ni-Al phase diagram after determining the Ni and Al activities at the composition range of 8-32 at% Al using KEMS. A more recent study [25] focused on the Ni-Al-Cr ternary system. In the present study, KEMS measurements were performed for temperature range within the relevant γ+γ' two-phase region of three single crystal superalloys, which were determined using DSC measurements. Samples for each alloy were analysed using SEM, revealing the microstructures formed during the KEMS measurement. It is found that just four of the alloying elements (Ni, Co, Cr, Al) have sufficient vapour pressure, detectable by KEMS.

Theory and Experimental set-up of Knudsen Effusion Mass Spectrometry

The Knudsen Effusion Mass Spectrometry (KEMS), although long established, is not very widely used in the metallurgical research community. The following section therefore presents a short introduction into the background of KEMS.

1. Activities

The activity $\boldsymbol{a_i}$ is this thermodynamic property that describes the chemically effective molar-fraction of its species $\boldsymbol{i}$ in a system (i.e. the solid solution). It is strongly affected by the nature of the species, its concentration and its interaction with other species in the system. A relation

describing the dependence of activities with the chemical potentials at equilibrium μ_i' and before the change occurs, $\boldsymbol{\mu_i}$ [26-29] is as following:

$$\boldsymbol{\mu_i}' = \boldsymbol{\mu_i} + \boldsymbol{lna_i} \quad (\mathbf{1})$$

Under equilibrium and ideal gas state, the activity of each element, can be defined as the ratio of its partial pressure over the system and the saturated vapour pressure when the element is found in its pure form, solid or liquid, at the same temperature [27-30]. In the present work activities are defined in this way.

2. Background on Knudsen Effusion Mass Spectrometry - KEMS used in these studies

KEMS allows measuring activities through the analysis of vapour above a material sample. The composition of the vapour, which is in equilibrium with the condensed material, is characteristic of the activities of volatile elements in the sample. Generally, the apparatus for KEMS measurements consists of a Knudsen cell, a pyrometer, which measures the temperature on the surface of this cell, an ion source and a mass analyser (**Fig.1)**. A sample in condensed phase is placed inside the Knudsen cell and kept at constant temperature and high vacuum. A very narrow orifice on top of the cell allows a small amount of vapour to effuse without disturbing solid-gas equilibrium within the cell. The effused molecular beam is regarded as leading to an infinitesimal small reduction of the initial mass of the sample in the cell. The relative fraction of the species in the effused beam of vapour is identical to the relative fraction of the species in the vapour within the cell. The molecules in the vapour stream are then ionised using electrons emitted at constant rate (e.g. 0.50 mA) and defined energy ***E*** (e.g. 70 eV). These ions are accelerated in an electric field so that they show identical energies before entering the analyser. Finally, detectors are measuring the intensities (i.e. count rates) of each type of ion found in the gas stream. In the present work 'intensity' will be used as a shorthand term for 'the ion counts of the corresponding components'.

In order to determine the activity of species $\boldsymbol{i}$ in a multicomponent system, KEMS measurements are conducted within a defined temperature range for:

i) the multicomponent system with species $\boldsymbol{i}$ present and
ii) the pure compound with the same species $\boldsymbol{i}$

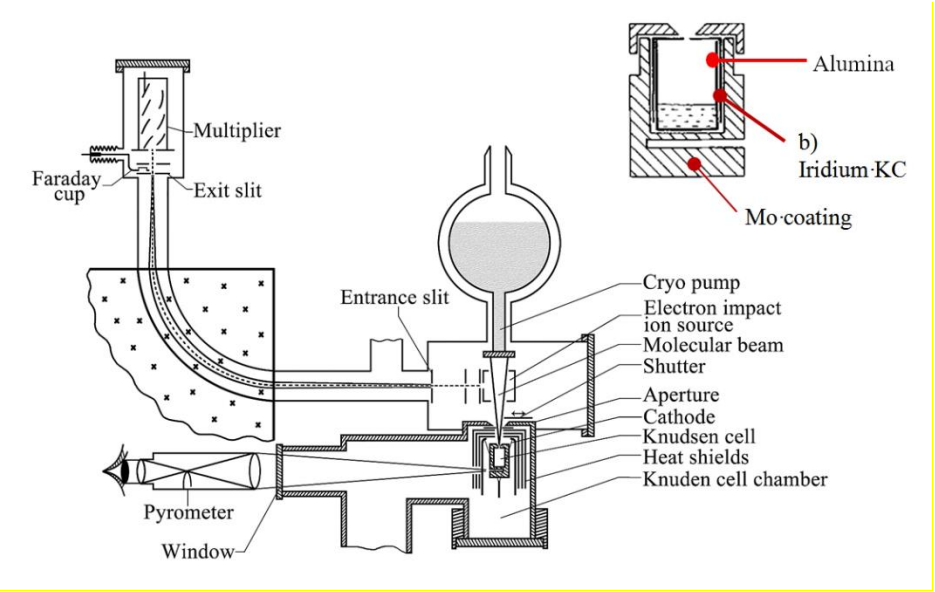

***Figure 1**: Schematic representation of KEMS [31, 32].*

The resulting intensities $\boldsymbol{I_i}$ and $\boldsymbol{I_i^0}$ of species $\boldsymbol{i}$, in the multicomponent system and its pure form respectively, are obtained by successively heating (or cooling respectively) to and holding at a temperature within a defined temperature range. Holding assures that thermodynamic equilibrium is established before measurements are taken. The measured intensities are proportional to the partial pressures $\boldsymbol{p_i}$, as expressed by equations 2 and 3 [14-19, 21, 32-38]:

$$\boldsymbol{p_i = \frac{k I_i(E) T}{n_i \sigma_i(E)} = B\, I_i(E) T} \qquad (2)$$

Where $\boldsymbol{k}$ is an instrument constant, $\boldsymbol{n_i}$ the isotopic abundance of element $\boldsymbol{i}$, $\boldsymbol{\sigma_\iota}$ is the ionization cross section, at the electron ionizing energy $\boldsymbol{E}$ and $\boldsymbol{B}$ incorporates the isotopic abundance, ionization cross section, and instrument constant.

The energy of the measured counts is known and is lower than 10 eV. The ion efficient curves are nearly constant for all elements at 70 eV, according to standard knowledge for KEMS studies [38]. Thus, in the present work the electron ionizing energy $\boldsymbol{E = 70\ eV}$ is used [37-39].

Ionisation cross sections have been measured and determined [34, 37] and calculated using quantum methods [38, 40]. However, obtaining accurate cross sections is still one of the main challenges for KEMS method and more work needs to be done in this area. **Equation 2** provides a way to determine partial pressures directly from measured intensities of the corresponding species, but all quantities given in **equation 2** need to be very accurately

known. This is however quite difficult for reasons outlined above. An alternative approach is using the relation given in **equation 3**, which is derived from **equation 2** and the basic definition of elemental activity. For a given temperature the activity can be obtained as:

$$\boldsymbol{a_i = \frac{p_i}{p_i^0} = \frac{I_i}{I_i^0}} \quad (\mathbf{3})$$

Where $\boldsymbol{p_i^0}$ **and** $\boldsymbol{I_i^0}$ are the saturated vapour pressure and measured intensity, respectively of species $\boldsymbol{i}$ in its pure form.

The component activity in the metallic system, for which intensities are measured using the KEMS method, can be easily determined at a given temperature range (**equation 3**), provided that intensities of the corresponding pure element are also measured using the same experimental setup under the same conditions.

Other essential thermodynamic quantities can be derived from partial pressures and activities measured over temperature ranges. When solid $\boldsymbol{A}$ is found in its pure form, the corresponding reaction constant becomes [28, 29]:

$$\boldsymbol{K_p = \frac{[p_{A(g)}]^{\nu_j}}{[a_{A(s)}]^{\nu_i}} = [p_{A(g)}]^{\nu_j}} \quad (\mathbf{4})$$

By using the Clausius–Clapeyron equation, the equilibrium constant of the reaction of sublimation can be described as a function of the occurring enthalpy change $\boldsymbol{\Delta H}$ at a median temperature $\boldsymbol{T_m}$ [15, 16, 31, 33, 41]:

$$\frac{d\boldsymbol{lnK_p}}{d(\frac{1}{T})} = -\frac{\boldsymbol{\Delta H}_{T_m}}{R} \quad (\mathbf{5})$$

where $\boldsymbol{R}$ is the gas constant.

Thus, the enthalpy change of sublimation can be determined from the following equation:

$$\boldsymbol{\frac{dln(I_iT)}{d(1/T)} = \frac{\Delta H_{T_m}}{R}} \quad (\mathbf{6})$$

Alternatively, the standard Gibbs energy of reaction $\boldsymbol{\Delta G^0_{(T)}}$ is obtained from the equilibrium constant using **equations 7 and 8**:

$$\boldsymbol{\Delta G^0_{(T)} = -RT\, lnK_p = \Delta H^0_{(T)} - T\,\Delta S^0_{(T)}} \quad (\mathbf{7})$$

The Arrhenius plot links the reaction constant $\boldsymbol{lnK_p}$ with both the enthalpy and entropy changes due to sublimation or vaporisation:

$$\boldsymbol{lnK_p = -\frac{\Delta H^0_{(T)}}{R}\frac{1}{T} + \frac{\Delta S^0_{(T)}}{R}} \quad (\mathbf{8})$$

From these, relations for the alloy system and pure species respectively are obtained:

$$\boldsymbol{K_{p_i} \sim [I_i T] \ or \ lnK_{p_i} \sim ln[I_i T]} \quad (\mathbf{9})$$

$$\boldsymbol{K^0_{p_i} \sim \left[I^0_i T\right] \ or \ lnK^0_{p_i} \sim ln[I^0_i T]} \quad (\mathbf{10})$$

The reaction enthalpy can be determined from the slope of the Arrhenius plot over a well-defined temperature range ΔT. The intercept with the $^1/_T$ axis yields the reaction entropy change ΔS. Studies in the open literature about the systematic errors of the obtained results suggests that determination of the entropy of reaction requires more accurate measurements than are necessary for measuring the enthalpy of reaction [42]. In the present work, the uncertainty of temperature measurement is estimated around up to ± 5 K. Also, the material analysed is quite complex in composition. Hence, the measured results are used to determine enthalpy of reaction in order to evaluate the calibration of the experimental setup. The results are however regarded as not sufficiently accurate to determine the entropy of reaction, as slight change in enthalpy will lead to large changes in entropy, thus increasing the error in the entropy beyond reasonable limits.

Similarly, the activity $\boldsymbol{a_i}$ is related with the partial molar enthalpy $\boldsymbol{\Delta_m \bar{H}_i}$ and entropy $\boldsymbol{\Delta_m \bar{S}_i}$ of mixing of the alloy species $\boldsymbol{i}$ from the following equation:

$$\boldsymbol{\mu_i = RT\ ln\alpha_i = \Delta_m \bar{H}_i - T\Delta_m \bar{S}_i} \quad (\mathbf{11})$$

Thus, the molar enthalpy and entropy of mixing can derive from the variation of the logarithm of activity versus inverse temperature [20, 43].

Methods

1. Material and Sample Preparation

Three alloys were analysed with the method of KEMS: CMSX-4, CMSX-10K, and CMSX-10N. At room temperature all three alloys from two-phase microstructures consist of the disordered γ phase (fcc) and precipitates of the ordered γ' phase (L12). The γ' volume percentage can reach up to 80%. Upon heating the γ' phase disappears at the γ' solvus temperature and all three alloys show a single phase γ microstructure up to the solidus temperature where the material starts melting. The single-phase region between solvus and solidus temperature is commonly referred to as the solution heat treatment window. It is fairly wide for CMSX-4 and quite narrow for the CMSX-10 alloys. Details of the transition temperatures are discussed in the DSC 'Results' section. The compositions of all three alloys were measured using Inductively Coupled Plasma Optical Emission Spectroscopy (ICP-OES Analysis) and the nominal compositions can be found in **Table 1**. Compositions were measured by dissolving samples in 50 ml HCl, HNO_3, and HF. Concentrations of all elements were then measured at various dilutions. The alloying element measurement was carried out using matrix matched calibration. Three spectrum lines were used for evaluation for all elements. Overall, it was found that the compositions of all three alloys is very close to the corresponding nominal compositions: deviations where typically between 0.1 wt% and 0.2 wt%. Summing up the concentrations of all alloying elements, the total percentages of unidentified impurities was found to be 1.46, 0.78 and 0.72 wt% for CMSX-10K, CMSX-4 and CMSX-10N, respectively.

Samples for KEMS and DSC studies were prepared following identical routes. All material was taken from directionally solidified single crystal material of cylindrical in shape (8 mm diameter and 65 mm length), which had undergone industrial standard, proprietary solution heat treatment and ageing, comparable to the solution heat treatment described in Ref [44]. All samples were then mechanically polished by surface reduction of around 0.5 mm to eliminate any surface modification inherited from industrial processing. Subsequently, pie-shaped wedges were cut from each cylinder by Electrical Discharge Machining (EDM), (AgieCharmilles CUT 20 P, supplied by GF Machining Solutions). These wedges were then cross sectioned into thin slices of around 2.5 mm thickness using a SiC cutting disc. In order to avoid interference from residual oxide scale during KEMS measurements, samples were broken into two pieces after being filed with a diamond file. Only one of these halves was used during KEMS measurements. The other half was kept as the reference sample for microstructure analysis.

Table 1: Composition of CMSX-4, CMSX-10K and CMSX-10N.

Alloy	Al	Ti	Cr	Co	Mo	Nb	Hf	Ta	W	Re	Ni	
	wt%											
CMSX-4	5.6	1.0	6.4	9.7	0.6	-	0.1	6.5	6.4	3.0	60.7	Nom. [45]
	5.81	1.0	6.3	9.29	0.6	0.02	0.1	6.53	6.23	2.84	60.5	**ICP-OES**
CMSX-10K	5.8	0.2	2.3	3.3	0.4	0.1	-	8.3	5.5	6.3	67.8	Nom. [46]
	5.7	0.21	2.17	3.21	0.39	0.1	0.02	8.19	5.22	6.03	67.3	**ICP-OES**
CMSX-10N	5.9	0.1	1.7	3.1	0.5	0.1	-	8.5	5.5	6.8	67.8	Nom. [47]
	5.88	0.09	1.49	2.97	0.5	0.04	0.03	8.58	5.31	6.69	67.7	**ICP-OES**
	Nominal composition in at%											
CMSX-4	12.3	1.3	7.6	10.3	0.4	-	0.1	2.5	2.5	1.1	61.9	
CMSX-10K	13.2	0.3	2.8	3.6	0.4	0.1	-	3.4	2.2	2.5	71.7	
CMSX-10N	13.5	0.1	2.1	3.4	0.4	0.1	-	3.5	2.2	2.6	72.2	

2. Knudsen Effusion Mass Spectrometry (KEMS)

2.1. Equipment and Temperature Calibration

The specifications of the Knudsen effusion mass spectrometer, including the pyrometer type are described in great detail elsewhere [32]. The ionisation electron energy and the emission current were set to 70 eV and 0.5 mA, respectively. The temperature was calibrated by monitoring the change in vapour pressure around the melting points of silver isotope ^{107}Ag, of 51.84% abundance at 1238 K ± 2 K and nickel isotope ^{58}Ni, of 68.27% abundance at 1726 K ± 2 K [48, 49]. Intensities were also measured in the liquid phase from 1343 K to 1523 K for the single isotope ^{197}Au, for which the enthalpy of vaporisation for the single isotope ^{197}Au was determined at 343.65 KJ/mol for the median temperature of 1433 K, after intensities were measured in the liquid phase from 1343 K to 1523 K. According to IvtanThermo [50], the vaporisation enthalpy of Au is 347.382kJ/mol, The SGPS database (version 13.1, revised in 2019) [51] suggests this is 347.411 KJ/mol. The value obtained by the present work is 4 KJ/mol lower compared to literature. This is within the ± 5 KJ/mol range that is usually acceptable. The accuracy of temperature calibration is very important for obtaining reliable thermodynamic measurements.

2.2. KEMS Measurements

An alumina crucible containing the sample was placed inside an iridium cell. The lid on the iridium cell was also made from iridium with an orifice of 0.2 mm diameter. The temperature ranges for KEMS measurements were restricted to the γ+γ' two phase regions, as the DSC results demonstrated that the γ-single phase region of the CMSX-10K/N alloys is too narrow

for meaningful KEMS measurements with risk of melting the material. Melting and subsequent solidification leads to formation of microsegregation and thus destroys the homogeneous microstructure. Intensities were therefore measured for detectable species by heating from a minimum temperature of 1453 K, up to a maximum temperature below the γ' solvus temperature. The corresponding temperature ranges for each alloy are shown in **Table 2**. After reaching the maximum temperature, measurements were repeated during a cooling cycle back to the starting temperature. A combined heating + cooling cycle was regarded as one measurement run. Each sample was tested for four complete runs of heating and cooling before being removed from the KEMS cell. During each run, temperature steps of either 10 or 20 K were used. When a new temperature was reached, measurements were preformed after an isothermal hold of 10 minutes.

Table 2: Temperature ranges for KEMS measurements of the samples under study.

	pure Ni	**pure Co**	**pure Cr**	**pure Al**
KEMS Temp. [K]	1399 - 1711	1430 - 1699	1406 - 1567	1147 - 1384
	CMSX-4	**CMSX-10K**	**CMSX-10N**	
KEMS Temp. [K]	1453 - 1513	1453 - 1573	1453 - 1548	

In order to determine which elements to analyse, preliminary KEMS measurements took place for each alloy, during which samples were heated to temperatures well above the solidus temperature (**Table 2**). The total mass spectrum was scanned during these measurements, with a focus on the isotopes Ni^+, Co^+, Cr^+, Al^+, and Ti^+. The measurements showed detectable vapour pressures for Ni, Co, Cr, and Al only, and therefore the work concentrates on these elements. In order to determine how much time is needed for the system to reach equilibrium, the signal of Ni was checked in the highest and lowest temperatures of each complete study, before starting with the KEMS measurements for a particular temperature range; i.e. with maximum temperatures lower than γ' solvus, at the two-phase region of γ+γ'. It was found that it takes up to two minutes before Ni^+ exhibits a steady signal, which then remained steady during the following 30 minutes of monitoring.

KEMS measurements were also taken for pure elements that were measured in the system of each alloy; pellets of 99.999% pure Cr and Al and 99.99% pure Ni and Co covering the sample temperature range as for the main measurements.

In order to determine the activities of the detected species in the alloys, the temperature dependent intensities were measured for pure Ni, Co, Cr and Al for the listed temperature

ranges in **Table 2**. The sublimation enthalpies for the median temperatures of these ranges, as seen in **Table 4,** are obtained from the slopes of Arrhenius plots (**Fig. 4**), according to **equation 5**.

3. Differential Scanning Calorimetry (DSC) Measurements

The objective of the DSC measurements was to determine the γ' solvus, the solidus and the liquidus temperatures of the alloys used in the KEMS study, so that the KEMS cycles can be planed accordingly. In order to achieve this, all samples had undergone solution heat treatment and only DSC traces taken upon heating were used. This ensured that microstructure and microsegregation inherited from previous solidification was if not eliminated, minimised. It should be noted that during a typical industrial Bridgman process, single crystal superalloys undergo cooling rates of the order of 12 K/min, which is comparable to cooling rates commonly used in a DSC. Hence, DSC cycles cooling from above the liquidus temperature can be regarded as nowhere near equilibrium.

The apparatus used in the present study was a DSC 404C type, supplied by Netzsch GmbH. It was used to determine the temperatures at which observable enthalpy changes occur within the temperature ranges used for KEMS measurements. The used DSC device is equipped with rhodium heating elements, capable to achieve a maximum temperature of 1923 K. Samples were placed in alumina crucibles of 85 µl volume, covered with matching lids with small orifices to allow high purity Ar gas of 100 ml/min flow rate insert each sample throughout each set of measurements. A vacuum system decreased the pressure down to 10^{-2} mbar, before backfilling with Ar at the start of each measurement, which was intended to minimize oxidation. The DSC instrument was calibrated for temperature and enthalpy with Palladium (Pd), Gold (Au), Silver (Ag), Aluminium (Al), Zinc (Zn), Indium (In) and Tin (Sn). All samples were weighted before and after the experiment and no weight change was observed. The micro-balance scale used for this purpose is supplied by Ohaus model PA64 [52] and allowed accuracy of 5 decimal points of 1 gram.

Three complete cycles of heating and cooling at ramping rates of 5, 10, 20 K/min for each of the alloys CMSX-4, CMSX-10K and CMSX-10N were performed. Studies started after each sample remained at 1373 K for 20 minutes, followed by ramping up to a maximum temperature of 1703 K for CMSX-4 and 1753 K for CMSX-10K and CMSX-10N. Maximum temperature was chosen to ensure complete melting of the samples. Cooling started after a 20-minute isothermal hold at the maximum temperature, down to 1373 K at the same rate as during the heating stage.

4. Observation with Scanning Electron Microscopy (SEM) - Energy Dispersive Spectroscopy (EDS)

A Scanning Electron Microscope / Energy Dispersive Spectrometry (SEM/EDS) of type Supra 50VP (supplied by Zeiss), was used to study the effect of KEMS on the microstructure of the alloys both at the bulk and at the surface, before and after KEMS measurements were complete. Back-scattered images were taken at 15 kV accelerating voltage and 10 mm working distance. The mounted surfaces were selected after optical assessment according to the roughest observed sides of the samples. After mounting, all samples were ground and polished to 1 μm (diamond grain size), followed by fine polishing on a vibration polisher (Al_2O_3, 0.05 μm) for two hours.

Results

1. DSC Measurements

The DSC method was used to determine the temperatures at which phase transitions with countable enthalpy change occur such as the solidus and liquidus temperatures. This is important for selecting appropriate temperature ranges for the KEMS measurements. DSC measurements during heating of homogenised microstructures resulted in determining the value of γ'solvus, which is the maximum temperature of the two-phase region γ+γ' before each alloy starts melting at the solidus temperature (**Table 3**). Micrographs depicting similar microstructures are presented further in this work for the bulk (**Fig. 12.a, 12.c, 12.e**) and surface (**Fig.13**). A reaction starts before melting, indicating the transition from the two-phase γ+γ' region into γ phase, depicted in **Figure 2** as γ' solvus temperature.

The values of temperature, where upon heating peaks corresponding to γ'solvus, solidus and the heating peak and heating offset occur at 5, 10 and 20 K/min for CMSX-4, CMSX-10K and CMSX-10N, obtained with DSC are extrapolated to 0 K/min as depicted in the plots of **Figure 3**. The values listed at **Table 3** correspond to the temperatures at 0 K/min after extrapolation.

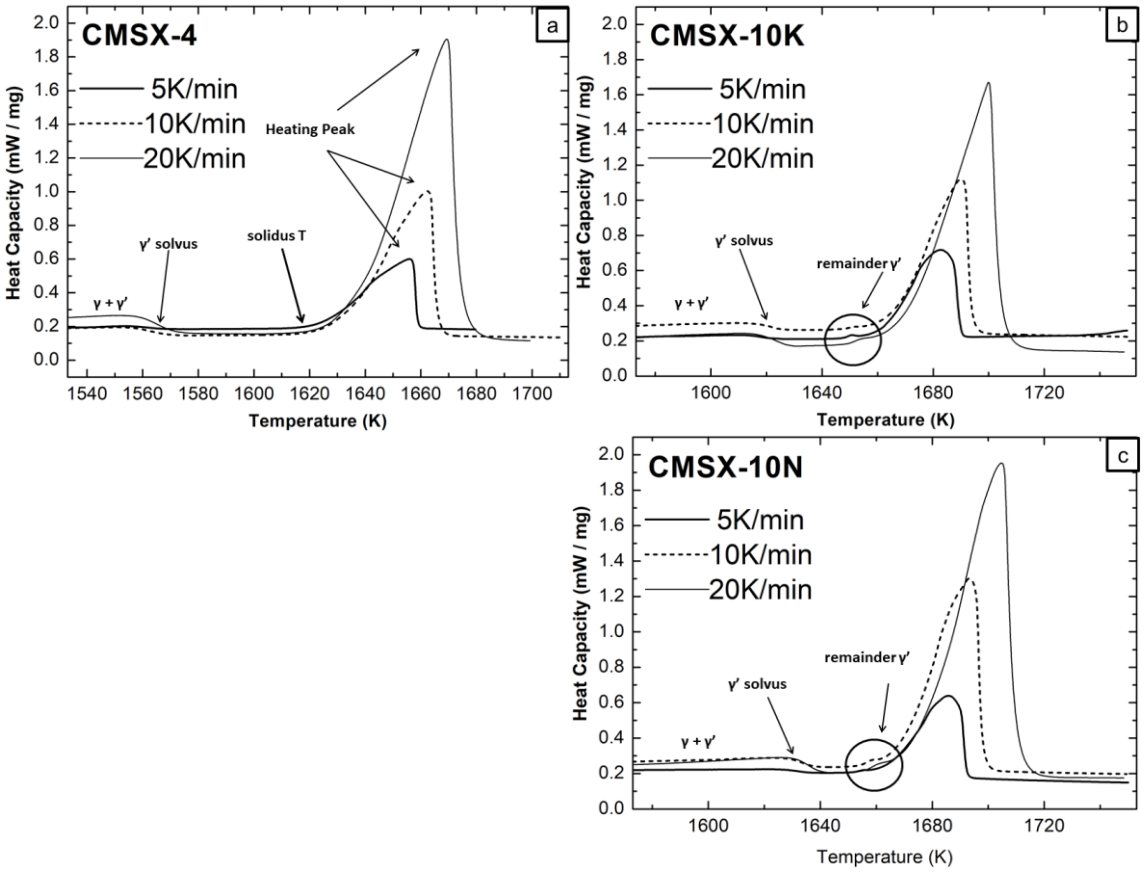

***Figure 2**: DSC results during heating at 5, 10 and 20 K/min of solution heat treated and primarily aged samples of alloys CMSX-4 (a), CMSX-10K (b) and CMSX-10N (c).*

The liquidus temperatures were determined from extrapolating temperatures for melting peak and the heating off-set, thus temperature ranges were obtained. For CMSX-4 this was found between 1653 K and 1655 K (**Fig. 3**). This range became wider for the other two alloys; 1678 K to 1688 K for CMSX-10K and 1680 to 1691 K for CMSX-10N, respectively.

In the present study, the heat treatment window is determined between the end of reaction (γ' solvus) and the start of melting (solidus temperature), [1556 to 1610] K for CMSX-4, [1605 to 1640] K for CMSX-10K and [1622 to 1649] K for CMSX-10N (**Table 3**). Observed solidus and solvus temperatures depend less on the DSC heating rate than the liquidus temperatures.

Table 3: Analysis of DSC results during heating after extrapolating to 0 K/min (**Fig. 3**).

	γ'solvus [K]	Solidus T [K]	Liquidus T [K]
CMSX-4	1556	1610	1654 ± 1
CMSX-10K	1605	1640	1683 ± 5
CMSX-10N	1622	1649	1686 ± 5

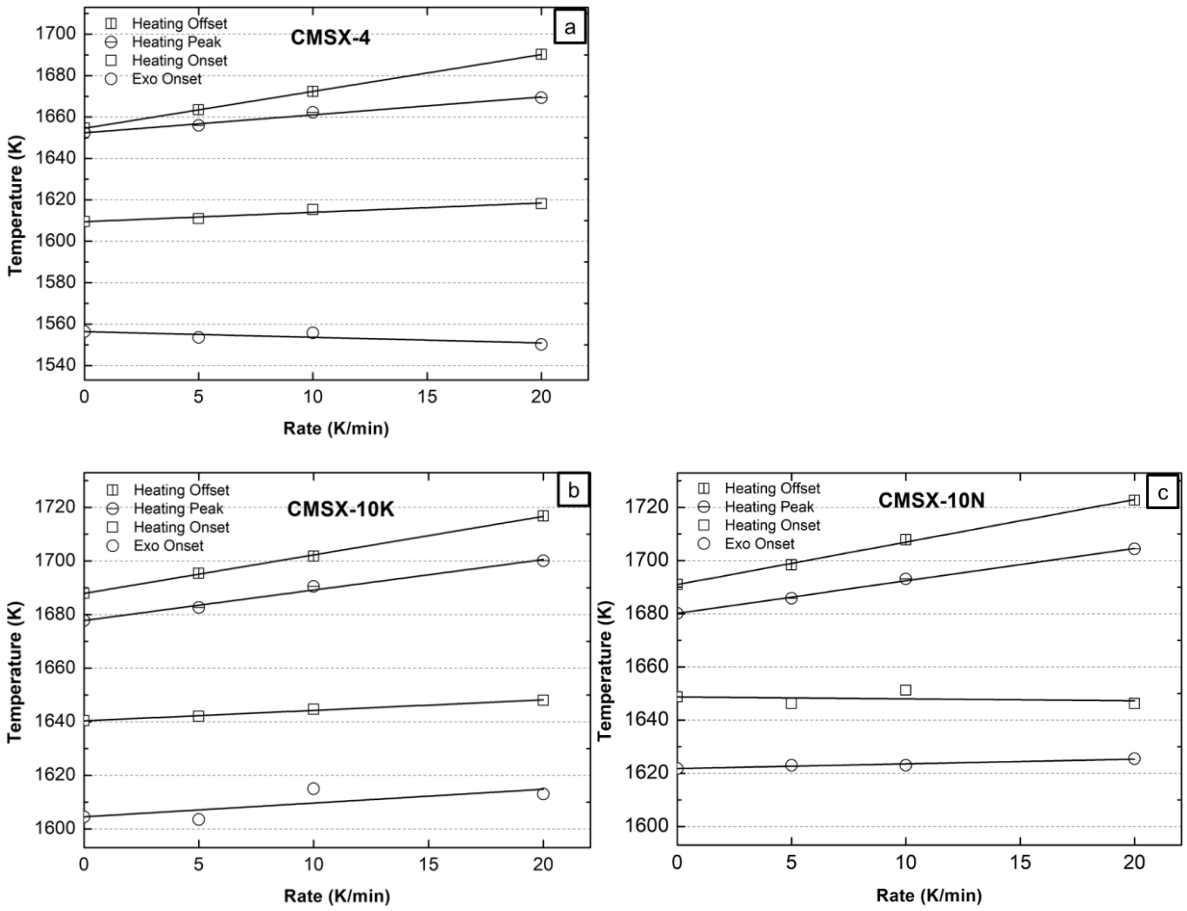

***Figure 3**: Extrapolation to 0 K/min of DSC results during heating at 5, 10 and 20 K/min of solution heat treated and primarily aged samples of alloys CMSX-4 (a), CMSX-10K (b) and CMSX-10N (c).*

2. KEMS Measurements

2.1. Mass Spectrum

Intensities of single-charged ions of the four isotopes Nickel $^{58}Ni^{+}$, Cobalt $^{59}Co^{+}$, Chromium $^{52}Cr^{+}$ and Aluminium $^{27}Al^{+}$ were measured during KEMS measurements. Starting from heating from a minimum temperature of 1453 K, up to a maximum temperature below the γ' solvus, four complete runs took place for each alloy. The intensities of double and triple charged ions of the corresponding abundant isotopes were also checked as well as the dimers Ni_2, Co_2, Cr_2. According to the mass spectrum, the masses of $^{85}(NiAl^{+})$, $^{117}(NiCo^{+})$, $^{110}(NiCr^{+})$ were also checked for each alloy at both high and low temperatures. The signal of titanium ions $^{48}Ti^{+}$ was very weak. The same occurred with the intensity of Ni^{2+} and Co^{2+} mass. Additional measurements took place for temperatures well above solidus temperatures. Intensities of the Ni_2^{+}, Co_2^{+}, Cr_2^{+} mass of 5%, 7.4% and 8.6%, compared to the corresponding single-charged ions for CMSX-10N, during these preliminary measurements have been detected at

1708 K. According to the results after analysing the data measured with DSC (**Table 3**), at this temperature CMSX-10N is completely liquid.

2.2. Measured Intensities

2.2.1. Determination of Sublimation Enthalpy of Pure Elements

Table 4 contains the sublimation enthalpies of pure Ni, Co, Cr and the vaporisation enthalpy of pure Al obtained from literature for the same temperature ranges as measured by KEMS.

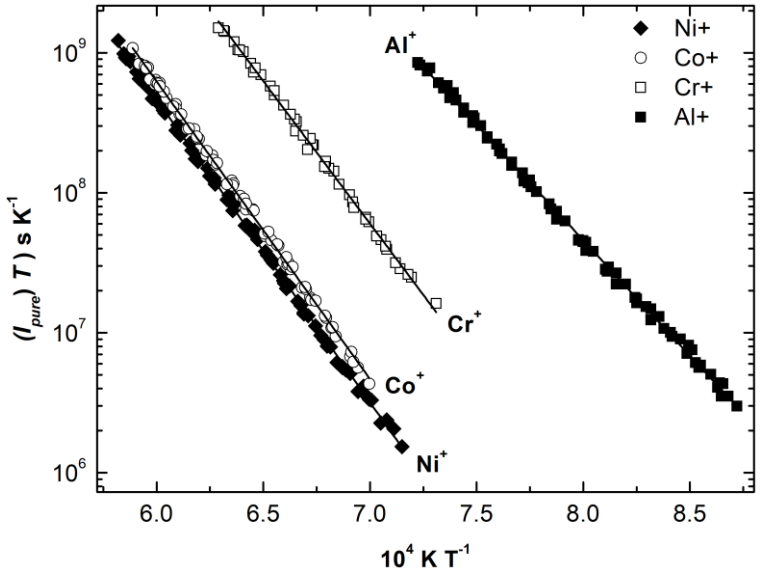

Figure 4*: Arrhenius plot of the measured ions with KEMS of the pure metals Ni, Co, Cr and Al.*

Linear regression on the Arrhenius plots of **Figures 4 and 5** yields with the corresponding slopes, which are proportional to the sublimation enthalpies. Uncertainties of the sublimation enthalpies include statistical uncertainties from the linear regression and a systematic uncertainty of ± 5 K on temperature values. The two sources of uncertainty are added in quadrature. The same procedure was used for the measurements in the alloys. In **Table 5** the standard deviation T (**sdT**) corresponds to the systematic uncertainty originated from temperature deviations, while standard deviation RS (**sdRS**) is the standard error derived from the linear regression. The width of the scatter band of measured intensities around the linear fit is 12%.

Table 4: Enthalpies due to sublimation of pure Ni, Co, Cr and vaporisation of pure Al (**equation 5**), as reported in the open literature.

	$\Delta_{sub}H$ / kJ mol^{-1}			$\Delta_{vap}H$ / kJ mol^{-1}
	Ni(s)	**Co(s)**	**Cr(s)**	**Al(l)**
IVTANTHERMO [53]	413.24 ± 2.0	410.65 ± 2.0	384.37 ± 2.0	309.32 ± 4.0
JANAF [54]	419.58 ± 8.4	413.50	384.89	309.28
Alcock [55]	421.52	418.97	383.64	310.354
Hilpert et al. [23]	423.56 ± 7.1			
Mean temperature T_m/K	1595	1573	1514	1406

2.2.2. Sublimation Enthalpy of Ni, Co, Cr, Al of CMSX-4, CMSX-10K and CMSX-10N

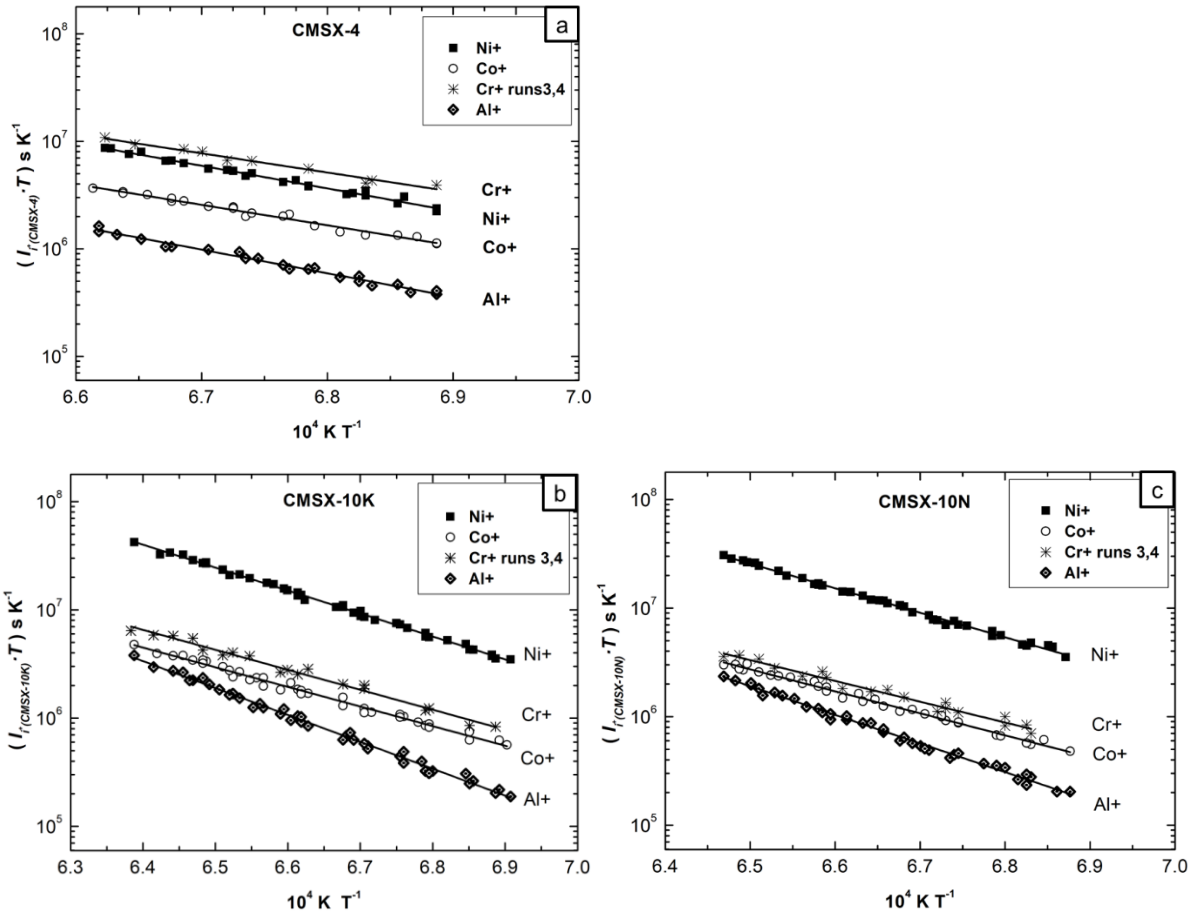

Figure 5*: Arrhenius plot of the measured ions of Ni, Co, Cr and Al, using KEMS, within* the two-phase γ+γ' region of alloys *CMSX-4 (a), CMSX-10K (b) and CMSX-10N (c).*

Four runs of KEMS measurements took place for each of the three alloys, starting from 1453 K up to temperatures below γ' solvus temperature. This upper limit was determined, for all three alloys, by DSC measurements (**Table 3**). For CMSX-10N, it was 1553 K, much lower than the γ' solvus at 1621 K. It was 31 and 33 degrees lower than the γ' solvus for CMSX-10K and CMSX-4 respectively.

Figure 5 depicts the graphical representation of KEMS results for Ni, Co, Cr and Al, for the alloys CMSX-4, CMSX-10K and CMSX-10N respectively, by plotting measured intensities as functions of reciprocal temperature. Measured intensities were at the same level for Ni, Co and Al throughout all four runs, while for Cr only runs three and four yielded comparable intensity levels. It is believed that this is due to microstructure changes near and at the surface of the material. Micrographs, as shown in a later section of the present work, do depict differences between the bulk and surface later after KEMS runs. It is interesting to see that these changes only have an effect on the intensities of Cr. The analysis of the data therefore used only Cr results obtained from runs three and four. The sublimation enthalpy obtained from the slope (**equation 6**) of the Arrhenius plots for Ni shows very similar results for all three alloys. This is explained, given the high concentrations in all three alloys in Ni; at 60.7 wt% in CMSX-4 and 67.8 wt% in CMSX-10K and CMSX-10N.

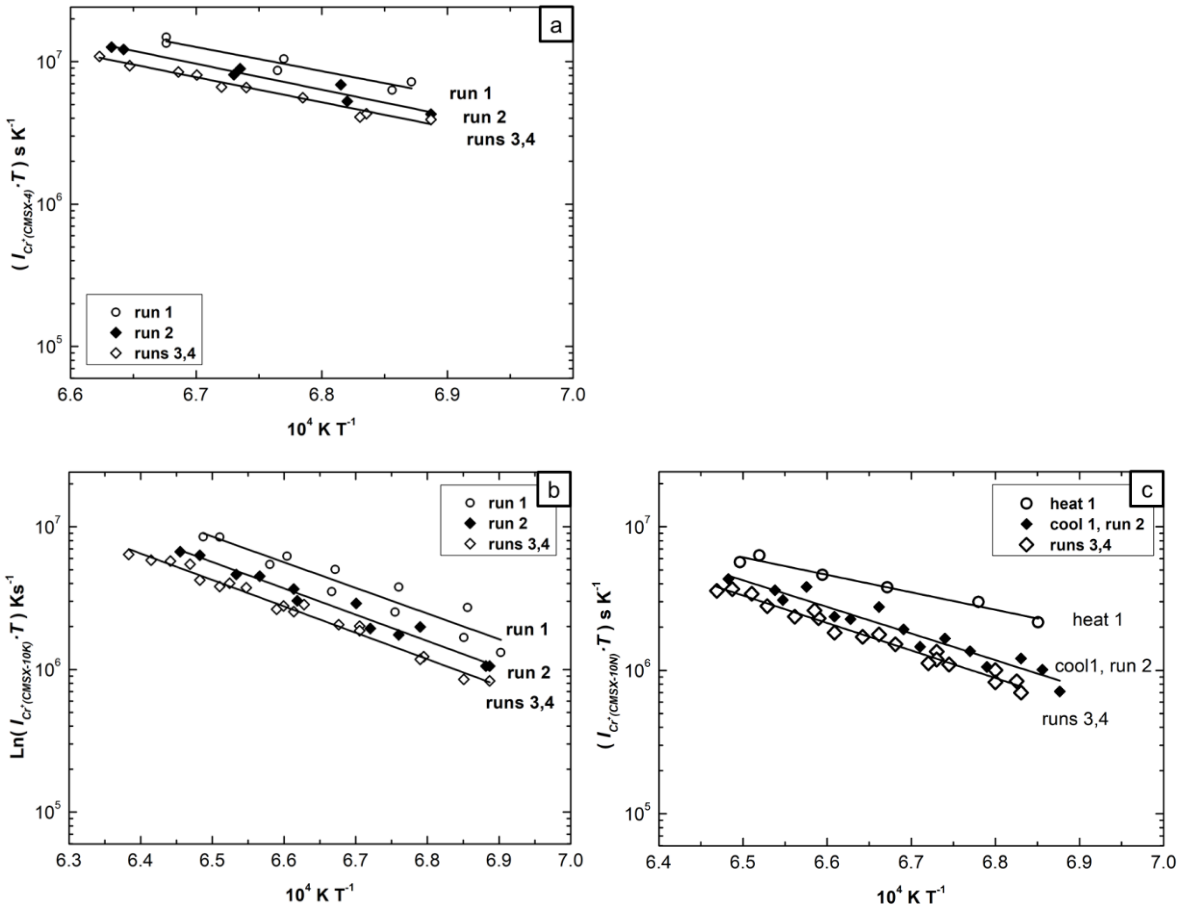

Figure 6*: Arrhenius plot of the measured Cr ions using KEMS within the two-phase γ+γ' region of alloys CMSX-4 (a), CMSX-10K (b) and CMSX-10N (c).*

Despite the composition of CMSX-4 being very different from the ones of CMSX-10K and CMSX-10N, the data measured for Ni, Co and Al was reproduced in each run. This is not the case for Cr, for which the activity is more difficult to determine, since the intensities of the ion

counts are changing from the first run towards the last by decreased values observed at both higher and lower temperatures.

The results for Cr in the three alloys are scattered among the different runs (**Fig. 6**). During the first cooling of the first run, intensities are found to be higher compared to other stages of both heating and cooling. It is observed that intensities of chromium are stabilised during the full duration of the third and fourth run. The corresponding value for the enthalpy of chromium is obtained after the linear regression of measured data during the last two runs 3 and 4. In the first two runs, the vapours of chromium exhibit a non-stable, non-reproducible behaviour during heating and cooling of each run.

Table 5: Sublimation enthalpies of Ni, Co, Cr and Al for CMSX-4, CMSX-10K and CMSX-10N and of the corresponding pure elements (**Fig. 5**, **equation 5**).

	$\Delta_{sub}H$ / kJ mol^{-1}			$\Delta_{vap}H$ / kJ mol^{-1}
	Ni(s) pure	**Co(s) pure**	**Cr(s) pure**	**Al(l) pure**
KEMS	**414.2 ± 2.9**	**406.4 ± 3.2**	**390.9 ± 3.9**	**315.7 ± 2.9**
Standard deviation **T**	± 2.6	± 2.6	± 2.6	± 2.5
Standard deviation **RS**	± 1.3	± 2.0	± 2.8	± 1.4
Mean temperature T_m/K	1555	1564.5	1486.5	1265.5

	$\Delta_{sub}H$ / kJ mol^{-1}			
	Ni(s)	**Co(s)**	**Cr(s)**	**Al(s)**
CMSX-4 (T_m/K: 1481)	403.7 ± **10.4**	364.7 ± 12.0	342.6 ± 19.2	421.8 ± **12.4**
Standard deviation **T**	±2.7	±2.4	±2.3	± 2.8
Standard deviation **RS**	±10.0	±11.7	±19.0	± 12.1
CMSX-10K (T_m/K: 1507)	406.4 ± **4.3**	347.1 ± **6.6**	353.0 ± **10.8**	475.9 ± **7.1**
Standard deviation **T**	±2.7	±2.3	±2.3	±3.1
Standard deviation **RS**	±3.4	±6.2	±10.5	±6.4
CMSX-10N (T_m/K: 1501)	432.9 ± **5.3**	388.1 ± **7.1**	367.0 ± **14.0**	505.1 ± **8.2**
Standard deviation **T**	±2.8	±2.5	±2.4	±3.3
Standard deviation **RS**	±4.5	±6.6	±13.8	±7.5

The calculated standard deviation in **Table 5** and its breakdown to $\boldsymbol{stT}$ and $\boldsymbol{stRS}$ lead to some observations concerning the method followed for analysing the KEMS data. In the case of Cr for all three alloys the selected sample from which Arrhenius plots are studied were the least (only runs 3 and 4 were considered). The lowest deviation for Cr is observed in alloys CMSX-10K and CMSX-10N. The largest deviation in $\boldsymbol{stRS}$ is observed in Cr for CMSX-4. For this alloy, deviations for all species are much higher compared to the corresponding values for the other two alloys with the largest contribution obtained by the deviation due to the linear regressions ($\boldsymbol{stRS}$). The reverse is observed for the pure systems. I.e. the main contribution in deviation is observed from the uncertainties added due to temperature variations.

2.3. Activities

The Ni, Co, Cr, and Al activities are determined from the KEMS measurements by relating intensities from measurement on alloys to measured intensities of pure elements. Care must be taken that both of these two intensities were obtained at identical temperatures. It needs to be taken into account that intensities for pure elements and alloy were performed in separate runs. Even with the greatest care, it is impossible to obtain identical temperature during two consecutive runs. Eliminating this kind of temperature variation was achieved in two ways, the results of both are shown in **Figure 7** as black and red symbols, respectively.

The first type of analysis is using a fitted linear expression to represent results for pure elements, while using measured intensity-temperature data points for the alloys. This data is shown as black symbols in **Figure 7**. The second method uses linear fits for both, pure element and alloy results, shown as red symbols in **Figure 7**. The use of a linear fit for at least one series of results allows consistent interpolation between temperatures. By using a fit for the pure elements only, scatter in measurements for the alloys is preserved, while using fits for pure elements and alloy, all scatter is removed.

The **Co and Cr activities** are higher in CMSX-4 compared to the two other alloys, decreasing by increased temperature, as seen in **Figure 7**. This is a clear indication of the role of the actual concentration of each species in the system of the alloys to the values of the activities: CMSX-4 is richer in Cr and Co, compared to the other two alloys, by at least 6.7 and 4.8 at% (**Table 1**). The activity values of CMSX-10K are slightly higher than CMSX-10N, especially for Co. The difference is more pronounced at lower temperatures.

The Ni activity of CMSX-4 and CMSX-10K/CMSX-10N shows higher activity values for the CMSX-10 alloys. The scatter of data points (i.e. data points in black) (**Fig. 7**) for all three alloys suggests no specific variation with temperature but narrowing scatter bands as temperature increases. Interestingly the results obtained from using a linear fit to the alloy data shown different signs in the slope for different alloys. As in each case the trend is well in the middle of the scatter band, it can be concluded that this is an effect of the fitting process. The effect of concentration on the activities is more pronounced for the case of Ni than for other elements, with the lowest activity values occurring for CMSX-4, which shows about 10 at% lower Ni concentration compared to the other two alloys (**Table 1**, **Fig. 7**). Generally, the Ni activity in all three alloys is significantly higher than the activities of Cr and Co.

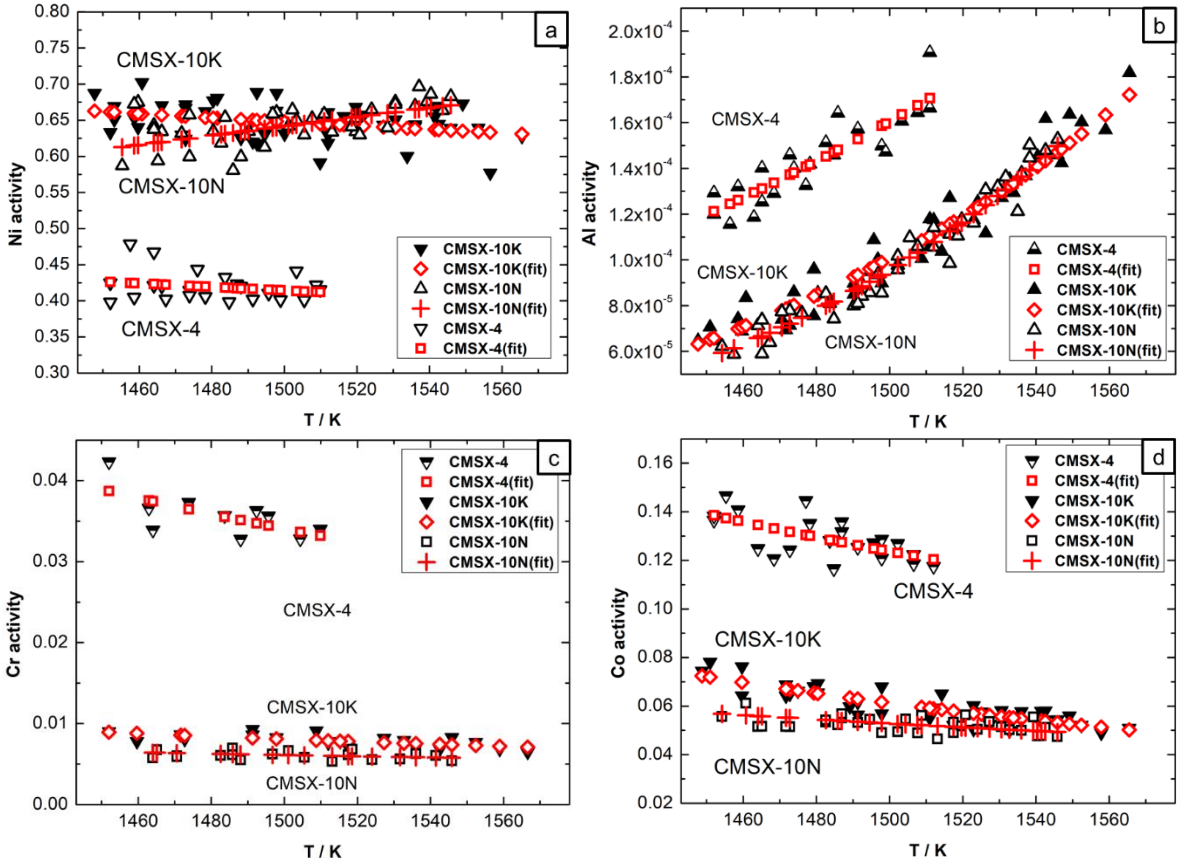

***Figure 7**: Activities of each species as a function of temperature is plotted concerning all three alloys for Ni (a), Al (b), Cr (c) and Co (d).*

The Al activity in all three alloys is about 3-4 magnitudes lower than the Ni activity, while showing a noticeable increase with temperature. Al activity in the CMSX-10 alloys is almost the same but is higher in CMSX-4. The concentration of Al in all three alloys is very similar: CMSX-4 is slightly lower with 12.3 at%, compared to 13.2 at% and 13.5 at% in CMSX-10K and CMSX-10N, respectively (**Table 1**). Despite its lower concentration, the Al activity is higher in CMSX-4, which clearly indicates thermodynamic interaction between alloying elements.

Figure 8 depicts the temperature dependence of activities for each of the three alloys. Activities are plotted at a logarithmic scale against the reciprocal scale of temperature. The plots reflect Arrhenius dependence for each element in each alloy. Using the measured intensities for the alloys in the plots of **Figure 8** and **equation 11**, we obtain the partial molar enthalpies of the corresponding species for CMSX-4, CMSX-10K and CMSX-10N at the median temperature of each dataset (**Table 6**). The uncertainty of each value is associated with the statistical error of the corresponding linear regression, multiplied with the gas constant $\boldsymbol{R}$. The obtained uncertainties are quite large, compared to the absolute values, which is due to the fact that data is obtained by scattered measured intensities. Determining

improved partial molar enthalpies and entropies would require additional KEMS measurements and possibly a different approach to KEMS measurements in multicomponent alloys.

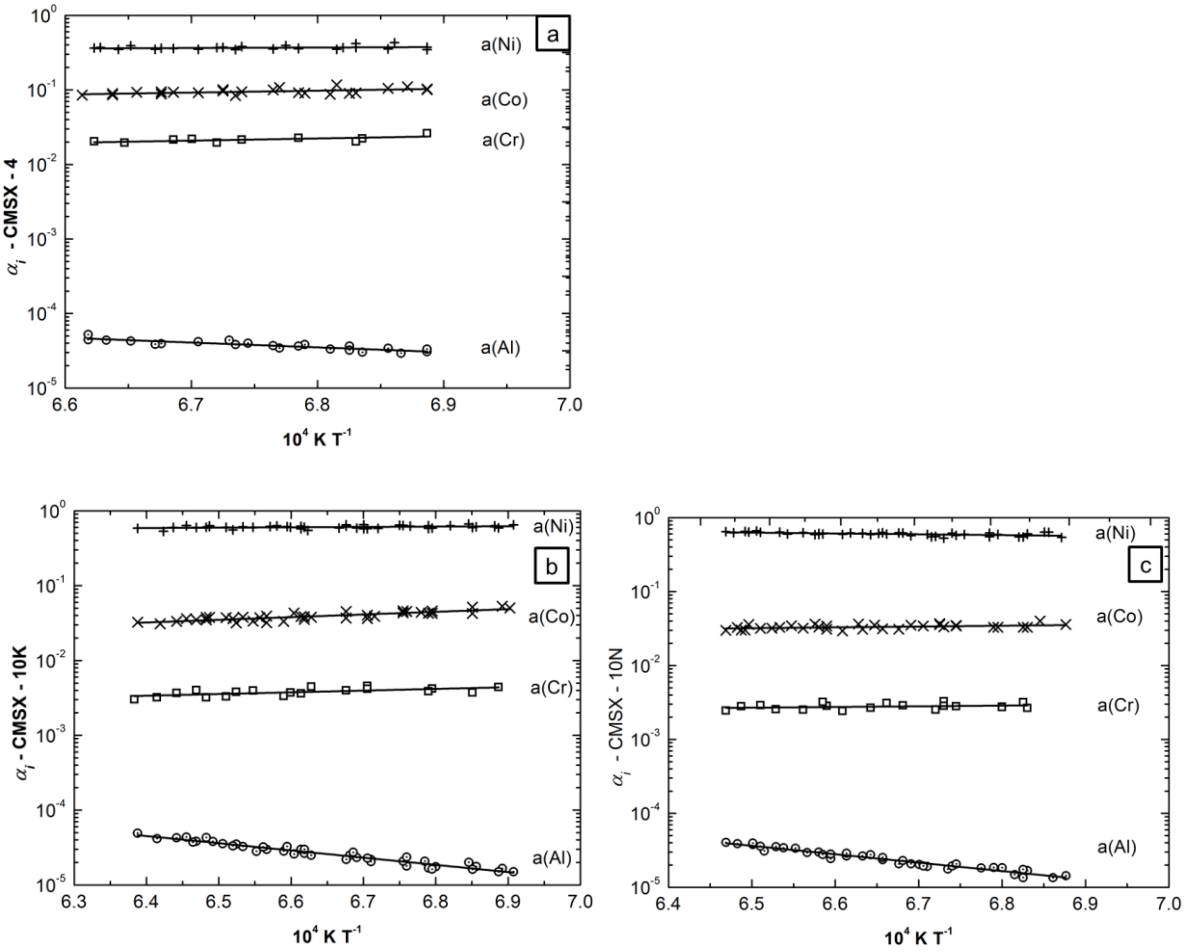

Figure 8*: Arrhenius plot of the activities for the species Ni, Co, Cr and Al using the intensities from KEMS measurements for CMSX-4 (a), CMSX-10K (b) and CMSX-10N (c). The temperature appears in reciprocal scale.*

Table 6[1]: Partial enthalpies of mixing of Ni, Co, Cr and Al in the alloys CMSX-4, CMSX-10K and CMSX-10N (**Fig. 8**, **equation 11**).

	i = Ni(s)	**i = Co(s)**	**i = Cr(s)**	**i = Al(s)**
CMSX-4 (T_m/K: 1481)				
$\Delta_{mix}\bar{H}_i$ / KJ mol^{-1}	10.6 ± 10.0	42.6 ± 13.2	48.4 ± 19.0	-107.4 ± 12.4
$\Delta_{mix}\bar{S}_i$ / J mol^{-1}K^{-1}	14.4 ± 6.8	45.8 ± 8.9	60.4 ± 12.8	1.0 ± 8.4
CMSX-10K (T_m/K: 1507)				
$\Delta_{mix}\bar{H}_i$ / KJ mol^{-1}	7.8 ± 3.4	59.3 ± 6.2	37.9 ± 10.5	-160.2 ± 6.4
$\Delta_{mix}\bar{S}_i$ / J mol^{-1}K^{-1}	8.8 ± 2.3	62.7 ± 4.1	65.4 ± 7.0	-30.3 ± 4.3
CMSX-10N (T_m/K: 1501)				
$\Delta_{mix}\bar{H}_i$ / KJ mol^{-1}	-18.6 ± 4.5	18.21 ± 6.6	15.4 ± 12.8	-189.3 ± 7.5
$\Delta_{mix}\bar{S}_i$ / J mol^{-1}K^{-1}	-8.7 ± 3.0	36.69 ± 4.4	52.8 ± 8.5	-49.2 ± 5.0

[1]Uncertainties due to standard error are included.

Figure 9 depicts the ratio of activities over the atomic fraction - taken from alloy composition - of Ni, Co, Cr and Al in the three alloys when only values from linear regressions have been considered. The ratios of Cr and Al are found to be almost identical when the two CMSX-10 alloys are compared, only very small differences are observed. Interestingly, the Al activity in CMSX-4 is significantly larger than the Al activity in CMSX-10K/N, despite the atomic fraction of Al being comparable in all three alloys. This can only be explained through the interaction of Al with other alloying elements. The results however obtained from the present work do not allow to establish which and how other alloying elements interact with Al to influence activities in this way. CMSX-4 has a higher atomic fraction of Co than CMSX-10K/N, thus the ratio between activity and atomic fraction of Co is lower in CMSX-4 than in the other two alloys. However, this is not the case for Cr, since the Cr activity in CMSX-4 is found much higher compared to the other two alloys.

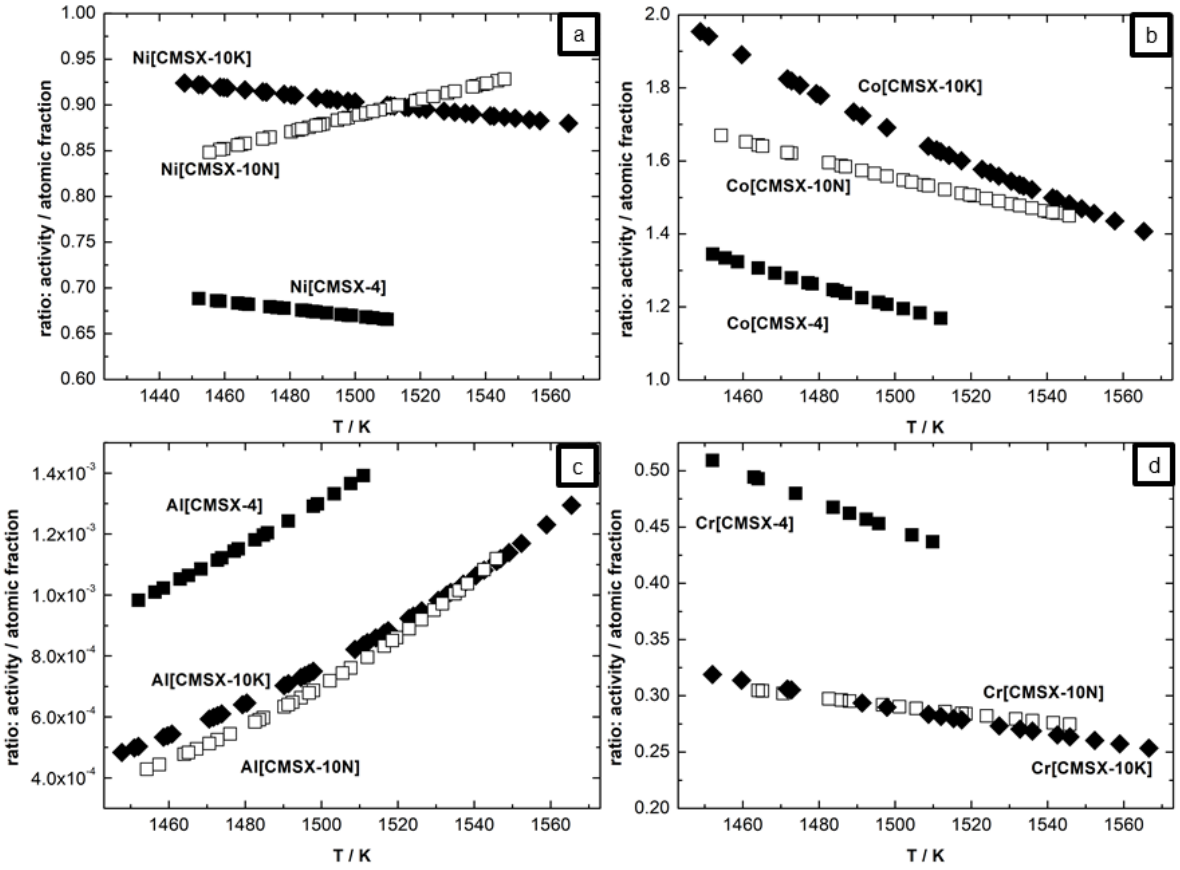

Figure 9*: Ratio of activity over atomic fraction of Ni (a), Co (b), Al (c) and Cr (d) is plotted against temperature for all three alloys.*

In the γ single-phase region this ratio would be the activity coefficient of each species and one could see the dependence of each component activity on its atomic fraction and whether this remains constant with temperature or even close to unity, i.e. following Raoul's Law. The plots are however showing the ratio in the γ+γ' two-phase region where phase fractions and thus phase compositions are changing with temperature. One can only understand that this

ratio doesn't change much for the same species at all three alloys, i.e. found at the same magnitude throughout the selected temperature range KEMS measurements took place. The graphs in **Figure 9** are still helpful, as they indicate influences due to interaction of chemical elements and thus excess Gibbs energy. Otherwise, all curves should collapse onto one curve. In parallel, changes in γ´ fraction with temperature might shift the curves temperature-wise.

3. Study of the Microstructure Post KEMS With SEM / EDS

Back-scattered images are used to analyse microstructures of prior and post KEMS treatment near the surface (**Fig. 10, Fig. 11**) and in the bulk (**Fig. 12**). EDS point measurements were done in order to determine the composition of different phases appearing in the images.

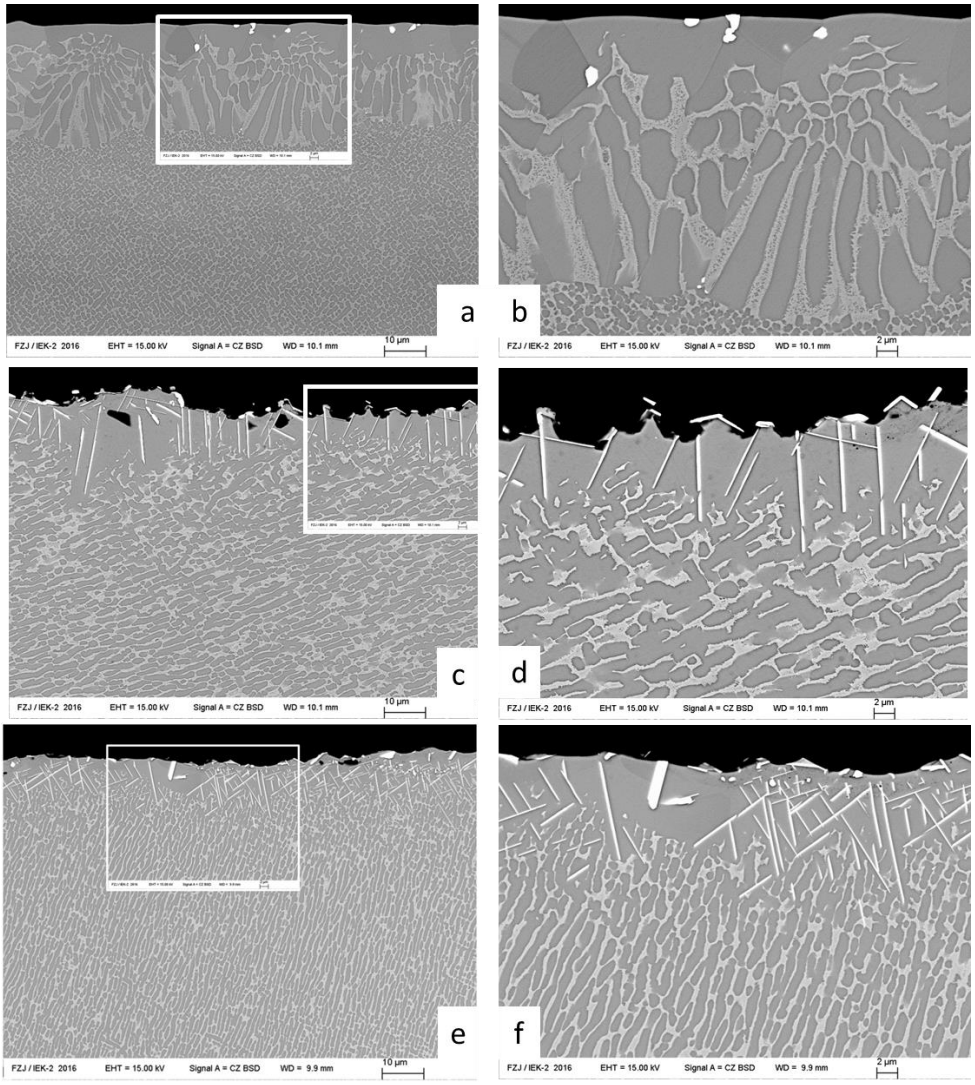

Figure 10*: Back-scattered images of surface modifications post KEMS for CMSX-4 (top:* ***a, b****), CMSX-10K (middle:* ***c, d****), CMSX-10N (bottom:* ***e, f****). Images enclosed in white frames in* ***a****,* ***c*** *and* ***e*** *are depicted in higher magnification in* ***b, d*** *and* ***f****, respectively.*

The surface of CMSX-4 exhibits a distinct, upper, thin surface layer of γ' grains decorated with white rounded small precipitates, indicating the presence of TCP phases (**Fig. 10b**). An intermediate layer can be found directly beneath, free from TCP phases, with characteristic lighter coloured waves into γ' matrix, indicating a mechanism of interdiffusion between the upper surface and the bulk. The surface modifications observed in CMSX-4 (**Fig. 10a**) are extended to depths of 20-30 μm and found larger compared to CMSX-10K (**Fig. 10c**) with 10-25 μm and CMSX-10N (**Fig. 10e**) with around 10 μm length. Nevertheless, at the surfaces of CMSX-10K (**Fig. 10d**) and CMSX-10N (**Fig. 10f**), no formation of grains can be identified using the back-scattered imaging, and there is not a clear distinction between the two layers of γ'phase as observed for CMSX-4 (**Fig. 10b**).

The TCP phase forming in CMSX-4 (**Fig. 10a, 10b**) is much coarser and smaller compared to the TCP observed in the other two alloys CMSX-10K ((**Fig. 10c, 10d**) and CMSX-10N (**Fig. 10e and 10f**). This distinction is similar to the observations reported by Rae et al. [56] at which μ and σ phases are described in detail when forming in CMSX-4 and RR3000 (same alloy composition with CMSX-10K), respectively. Comparison of micrographs obtained by this work indicates the presence of μ phase in the case of the alloy CMSX-4 (**Fig. 10a, 10b**). On the other hand, the fine needle-shaped TCP observed in the other two alloys, segregating around the γ' matrix, resemble the σ phase. The development of the latter phase is discussed by Suzuki et al. [57, 58] for the coated 4th generation Ni-based superalloys, after isothermal exposure at 1373 K for 500 hours. The micrographs obtained post KEMS of the CMSX-10 alloys depict similar behaviour on how fine needles of TCP, σ phase, coarsen around γ' matrix and grow towards the γ channels [56]. These channels look as the secondary phase in the bulk. The depicted microstructures look like the reversed two-phase γ+γ' microstructure observed at the micrographs of CMSX-4 (**Fig. 10a, 10b**).

Figure 11 depicts the surface on another side of the same CMSX-4 sample post KEMS. The outer layer consists of white needles and rounded precipitates rich in Re and W which are dispersed into grains of γ' matrix, indicating the presence of TCP phases. It is followed by a γ' zig-zag zone that sits between the outer layer and the inner area towards the bulk, free of grains and any other dispersed phase, separated clearly from the bulk without any trace of interdiffusion as in **Figure 10a** and **10b**. The microstructure of the inner area continuous towards the bulk with the same characteristics as observed in **Figure 12b.** The total length of the surface modifications is around 25 μm. **Table 7** contains the volume percentage of the TCP phases for the micrographs in **Figure 10 and 11**, obtained using ImageJ software [59]. The results in Table 7 however need to be treated with care. There is only a thin layer of material containing TCP phases on the surface of the sample, and only in some areas of the surface form TCP at a significant volume. The question that should be asked is whether the

composition in the TCP containing layer is homogeneous, and the answer is that it is -most likely- not.

Table 7: Volume percentage of TCP phases for micrographs in **Figure 10 and 11**.

Figure	Volume percentage of TCP phases
Figure 10b	0.43 %
Figure 10d	1.89 %
Figure 10f	3.08 %
Figure 11	4.02 %

EDS point measurements of separate phases, identified by different shades of grey colour, found almost identical composition for each phase in the back-scattered images. The darker coloured areas are rich in γ' forming elements Al, Ti and Ta, indicating γ' phase. Areas of lighter grey colour are found rich in W, Re and low in Al, Ti, and Ta indicating the composition of γ matrix. While the white coloured precipitates, rich in W and Re with very low content in Ni compared with other areas, are found without any Al or Ti present.

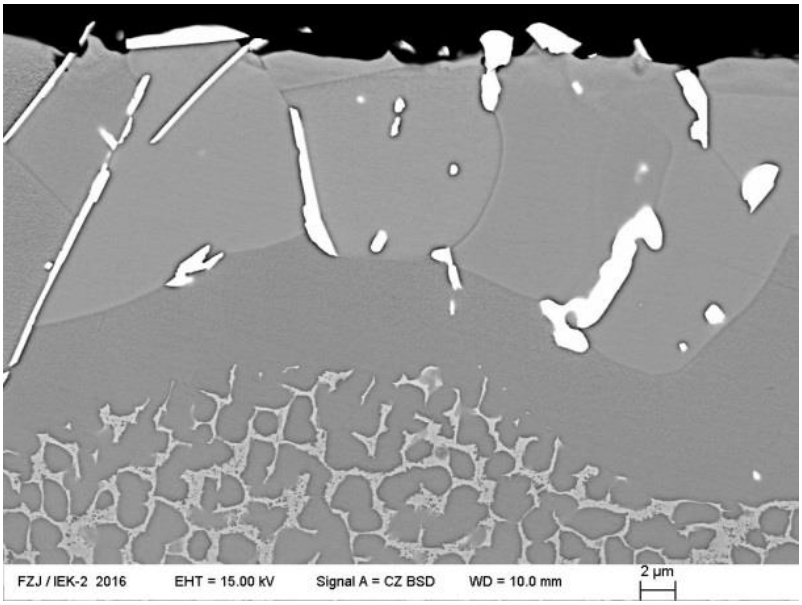

Figure 11*: Back-scattered image of CMSX-4 alloy with a unique surface modification post KEMS.*

Micrographs in Fig.12.a, 12.c and 12.e depict the alloys microstructure at the bulk, where Fig. 13 depicts the surface of alloys CMSX-4 and CMSX-10N of reference samples that have not undergone KEMS treatment. At the bulk of each alloy, the γ' precipitates, appear larger in CMSX-10K and CMSX-10N compared to those in CMSX-4 of around 2 µm post KEMS (**Fig. 12b, 12d, 12f**). Additionally, coarsening post KEMS is irregular in different areas to both CMSX-10K and CMSX-10N, with more pronounced effect in CMSX-10K (**Fig. 12d**) and

smaller precipitates of TCP phases of same composition as those seen close to the surfaces as shown in **Figures 10 and 11**.

Due to the very small scale of the observed surfaces with SEM/EDS, it was very difficult to monitor the exact surface that was exposed inside the KEMS cell prior KEMS measurements. An effort was made to study the surface directed from optical observation at the most non-uniform areas after KEMS treatment. However, additional processing due to metallography preparation may have removed information from the finally observed areas before those could have possibly been studied.

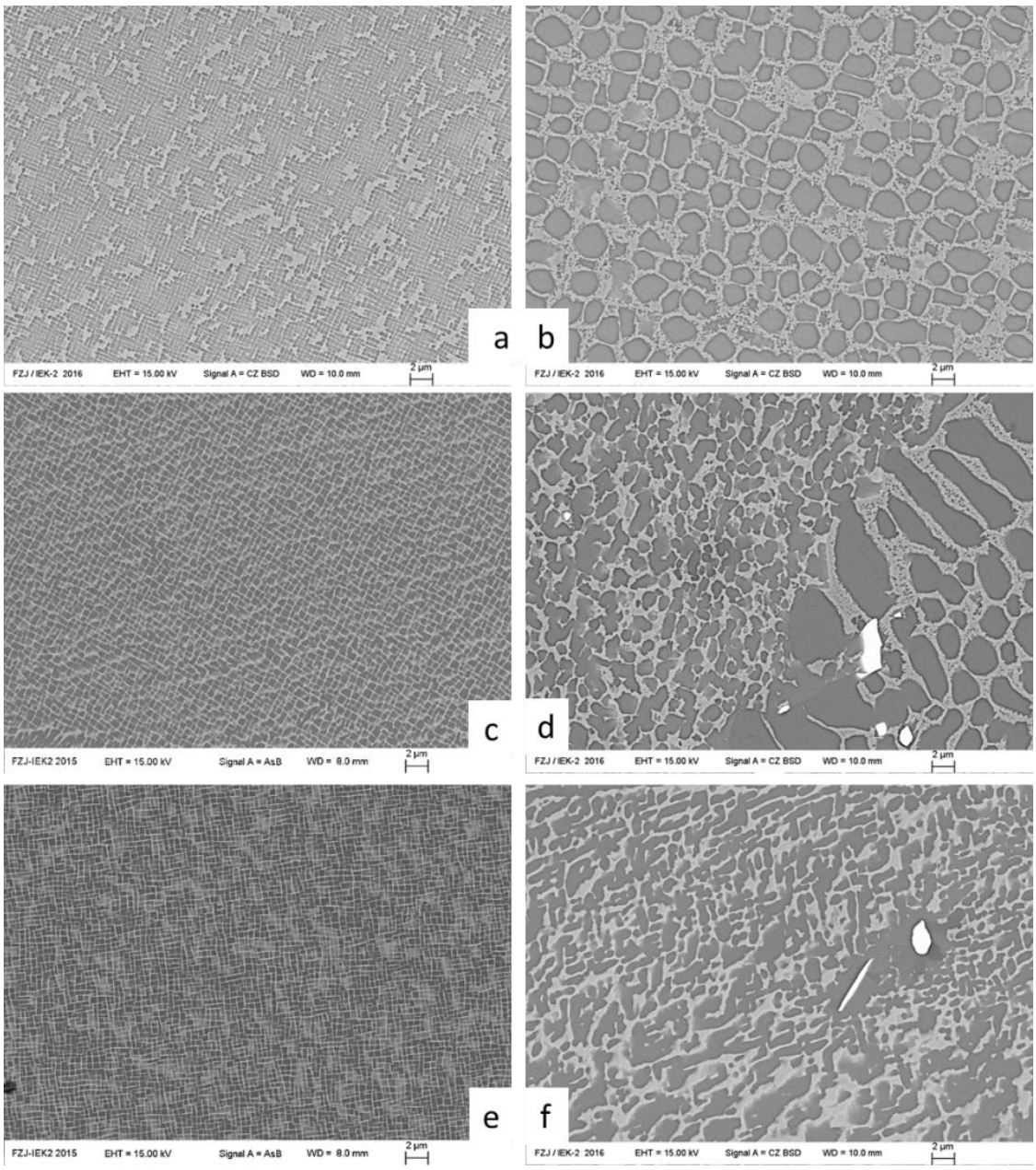

Figure 12*: Back-scattered images of bulk: CMSX-4 (**a, b**), CMSX-10K (**c, d**) and CMSX-10N (**e, f**). Left: Prior KEMS; fine precipitates of γ' with less than 0.5 µm size, dispersed into γ matrix of solution*

heat treated, primarily aged samples. The crystal structures are not perfect. Right: Post KEMS; coarsening of γ' precipitates, uniform in CMSX-4 and in more irregular configuration in CMSX-10K.

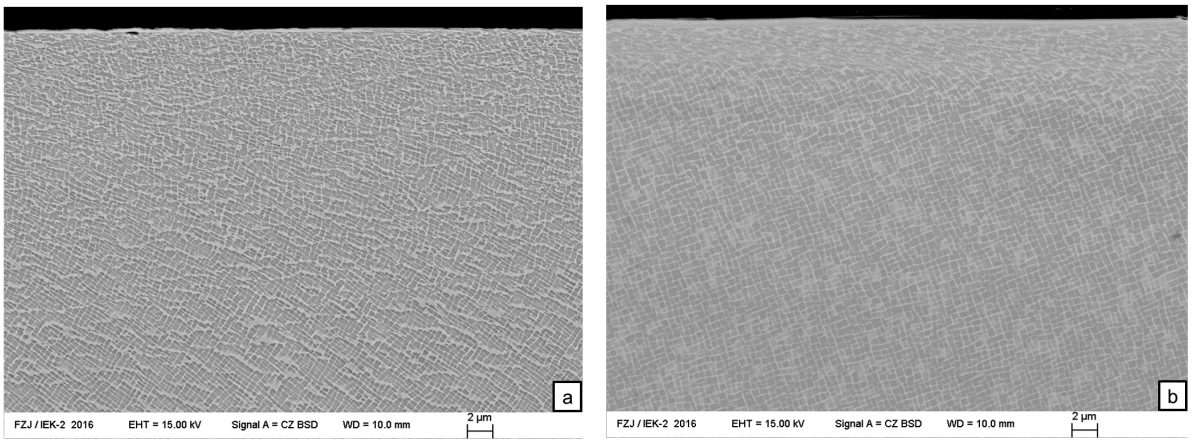

***Figure 13**: Representative back-scattered images of surface prior to KEMS measurements of CMSX-4 (a) and CSMX-10N (b).*

The images in **Figures 10-13** suggest that there are some changes, both at the bulk and on the observed surfaces. Overall, the images show a higher homogenous distribution of heterogenic phases. The microstructures at the bulk of each alloy are not changed significantly (**Fig. 12**), in contrast with the changes observed at the surface when comparing with micrographs in **Figure 13**. Coarsening in the bulk may occur due to the different rates of heating and cooling followed in KEMS and in comparison with the quenching conditions commonly followed when the microstructure is usually studied after heat treatments for the particular alloys [52]. The cooling stage after completion of measurements is assumed to be happening fairly fast. However, it is not possible to be achieved in similar rates to the quenching stage at heat treatment cycles. Additionally, the observed thickness of surface modifications are not the same at all sides of each sample, which do not exceed 25-30 μm, at the maximum.

Discussion

KEMS measurements were performed in the temperature range of [1453 -1573] K in the γ+γ', two-phase region, for the three alloys CMSX-4, CMSX-10K and CMSX-10N. These temperature ranges were selected after DSC measurements.

DSC measurements were complementary to the KEMS measurements. It is however interesting to see how the DSC results compare to data available from the open literature. The temperatures, at which phase transitions are occurring for the three alloys CMSX-4, CMSX-10K and CMSX-10N, were determined using DSC after extrapolation to heating rate of 0 K/min. For CMSX-10K, it is found that the γ' solvus occurs at 1605 K, solidus temperature at 1640 K and liquidus temperature at 1683 K ± 5 K. DSC measurements for the same alloy

by other study [46], performed during heating at 5 K/min, solidus temperature was determined at 1638 K, liquidus temperature at 1679 K and γ' solvus temperature at 1631 K. In a different study also at a heating rate of 5 K/min, the solidus temperature was reported as 1652 K [60]. Overall DSC results in the present study are within ± 2.5 K for solidus and liquidus temperature and ± 15 K for the γ' solvus temperature reported in other studies. It should be noted that the γ' solvus temperature is hard to determine via DSC as the signal is quite weak and smeared out over a temperature range. Hence, the DSC results are more than acceptable for the given purpose.

During the KEMS measurements, the vapour phase of four species, Ni, Co, Cr, and Al were detected. As a result, the activities of Ni, Co, Cr, and Al were determined for all three alloys as a function of temperature at this particular region. The observation that only these four elements sublimate is in agreement with the findings reported by Wang et. al. [61] for heat treatment of CMSX-10N. In their study, heat treatments were performed under Ar pressure of 2×10^{-4} bar, consisting of several ramp ups and isothermal holds up to a maximum temperature of 1623 K before quenching. They reported sublimation and condensation of Ni and Al as well as traces of Co and Cr.

In preparation for the present study, the ion intensities of the corresponding pure elements were measured with the KEMS method and the values of enthalpy changes are found in good agreement with literature data. The temperature calibration and the measured intensities from the experimental setup is therefore regarded reliable and accurate. Under these conditions, no traces of the elements Ta, W, Re, Ti, Mo, Nb or Hf were detectable in the vapour above the studied superalloys within the studied temperature ranges. It can therefore be concluded that vapour pressures of these elements were below the sensitivity of the mass spectrometer ($<10^{-9}$ Pa), and thus these elements do sublimate at a negligible rate, if at all.

The activities determined from the KEMS measurements show dependency on temperature and alloy composition. This is as expected. These alloys are quite complex however, and the different alloying elements are prone to influencing each other. On close observation, Ni shows the very little if any temperature dependency of activity. Ni constitutes >60 at% in all three alloys. The Al activity increases strongly at higher temperatures, while Cr and Co activities show slight decreases. The influence of composition generally follows expected trends, elements with higher atomic fractions show higher activities. The only exception is Al, which has a slightly lower atomic fraction in CMSX-4, but shows higher activity, compared to the other two alloys. This clearly indicates thermodynamic interaction of Al with other elements. The present data is too limited to work out which of the other elements causes this

effect in the Al activity. A full CALPHAD assessment could however shed some more light on this. Activities for each of the four sublimating elements in CMSX-10K and CMSX-10N are similar, which can be explained by relatively small differences in alloy compositions.

Previous studies have been reported for activities of Ni and Al in the Ni-Al system using KEMS [22, 23, 62, 63] and for the Ni-Al-O system, with a very low concentration of Oxygen (0.004-0.01at%) [24]. Oforka [62], Hilpert et al. [23] and Copland [24] have reported values of the activities of Ni and Al at mole fractions, comparable to the atomic fractions of Ni and Al in the CMSX-type alloys studied in the present work and at temperatures in the range of 1423-1600K, as shown in **Fig. 14** and **15**. The Ni activities measured for the CMSX-4/10 alloys are above those seen in the Ni-Al system, even though the Ni mole fractions are at comparable levels (**Fig. 14**). A similar but more extreme picture is seen for Al. **Figure 15** shows that in the studied alloys the Al activities are increased by a factor of 5 compared to Ni-Al binaries with comparable Al mole fractions. These results show that other elements in the three alloys (CMSX-4/10K/10N) interact with Ni and Al, leading to the observed activity increase. This means that the activity coefficient for Ni and Al is higher in the CMSX-4/10 alloys than in the Ni-Al binaries. Looking at a binary regular solution allows a simple analysis of the effect of elemental interaction on elemental activity. A positive regular solution coefficient indicates repulsive interaction between elements, and leads to activities higher than ideal. In the present study an increased activity coefficient therefore indicates that the net-interaction of both Ni and Al with the other elements in the alloys has to be more repulsive or at least less attractive than in the Ni-Al binary system. It has to be pointed out that from the data shown it is not possible to deduct specific interactions between individual elements, but only the interaction between Al/Ni and all other elements in the alloy as a whole.

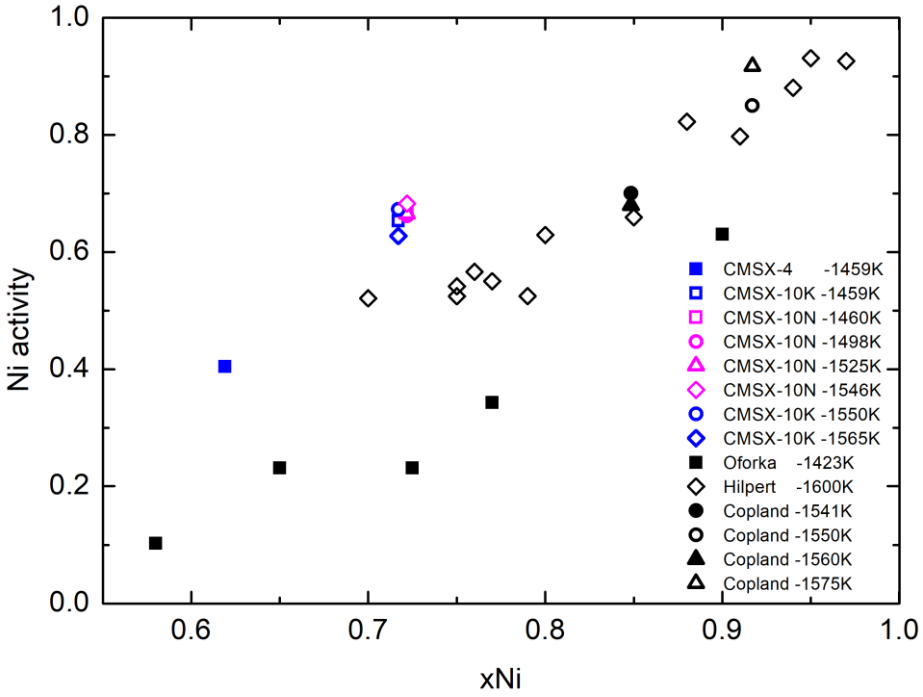

***Figure 14**: Data of Ni activity in the alloys CMSX-4, CMSX-10K and CMSX-10N compared with literature data using KEMS in the Ni-Al system in various temperatures.*

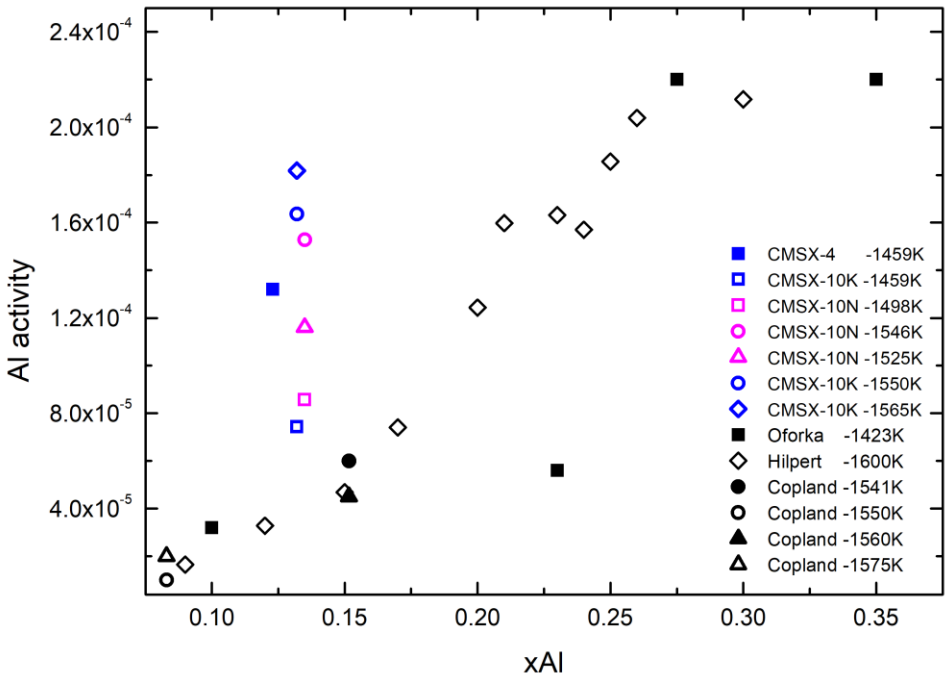

***Figure 15**: Data of Al activity in the alloys CMSX-4, CMSX-10K and CMSX-10N compared with literature data using KEMS in the Ni-Al system in various temperatures.*

In binary two-phase materials, the composition of both phases is fixed and connected by the tie-line, having identical activities. Hence, small changes of alloy composition will affect

phase fraction but not phase compositions or activities. In ternary or higher order alloys, changes in alloy composition lead to phase equilibria adopting different tie-lines. Hence, phase fractions and phase compositions will change. Activities will therefore be different even for small changes in the alloy composition. In the present study, only four out of ten alloying elements sublimate significantly. This will lead to changes of alloy composition at the surface of the material, which is partially compensated by diffusion. Diffusion in the metal and sublimation on the surface can be expected to happen at different rates until a dynamic equilibrium is obtained. The small changes seen between runs indicate that the material was indeed close to dynamic equilibrium.

The Ni, Co and Al activities appeared similar in all runs, but a noticeable variation was found for Cr. This was observed for all three alloys. Little variation was seen between repeated runs for Ni, Al and Co. It is found that the Cr intensities drop when measurements are repeated on the same sample, which is consistent with the atomic fraction of Cr dropping. The initial concentration of Cr is rather low, especially in the CMSX-10 alloys. So even small losses of Cr can have a significant effect on the Cr concentration, hence the observed changes between runs can be taken as indication of changes in the material during KEMS measurements.

KEMS is often regarded as a non-destructive method, as the amount of material sublimating from the surface is very, very small. Despite this, noticeable changes in the microstructure are observed, which are the result of alloying elements sublimating at different rates. The obtained microstructures post KEMS therefore reveal a different morphology in the surface layers compared to the bulk. Grains of γ’ phase have formed at the surface of CMSX-4 interspersed with TCP phases of rounded shape appearing on the grain boundaries. An intermediate layer, of about 20 μm length, consists of γ channels dispersed into γ’ matrix, interrupting the upper surface grains from the bulk. The microstructure of the other two alloys is different in the surface compared to CMSX-4. Long, needle-shaped TCP phases precipitate into γ’ matrix with extension of these needles into the γ+γ’ towards the bulk. This observation looks very similar to the microstructure of the Surface Reaction Zone (SRZ) for the coated 4th generation Ni-based superalloys, after isothermal exposure at 1373 K for 500 hours, as discussed by Suzuki et al. [57, 58].

It has been shown in a recent publication [64] that in the case of surface reaction accompanied by bulk diffusion, some elements diffuse faster than others. The present study suggests that Al diffuses fast enough from the bulk to areas close to the surface to compensate Al loss by sublimation. The change in composition over time leads to increased Al concentration at the surface. On the other hand, Cr and Co diffuse much slower from the

bulk to surface areas and are unable to compensate the effect of sublimation. At the same time, Ni sublimates, and as Ni is the solvent, the concentration of all elements in the alloy increases. This explains why γ' becomes the matrix of the microstructure in the surface layers, this layer is enriched in the γ' former Al and depleted in Cr and Co. Slow diffusion from the bulk is unable to replenish the γ forming elements Cr and Co in the depleted areas. The initial atomic fractions of these two elements are relatively low, as in the case of CMSX-10K and CMSX-10N. Due to the loss of these γ forming elements, the γ channels, as seen in CMSX-4 micrographs, are not found in the microstructures of the two CMSX-10 alloys. The other γ forming elements Re and W are enriched due to the loss of Ni and thus promote the formation of TCP phases. However, there is no information of when TCP phases started precipitating. Additionally, as also seen from the measured intensities and the values obtained for the activities (**equation 3**), the partial pressure of Cr is expected to be the highest of all four species (Ni, Co, Cr, Al).

The discussion above clearly indicates that the local composition change due to Cr coupled with processes in the material explains variations in KEMS measurements for Cr between different runs. The same applies however for Co, for which KEMS measurements through different runs are reproduced consistently for all three alloys. The difference between Cr and Co is primarily the different partial pressures and secondly their effect on TCP phase formation. Rae et al. [56] reported compositions of TCP phases, enriched in Cr, Re and W, as found at the substrate diffusion zones of aluminide and platinum-aluminide coated CMSX-4 and RR3000 (i.e. CMSX-10K). Cr is the only sublimating element that is also a TCP former. When TCP phases form, they absorb Cr, thus changing the Cr activity and Cr concentration in the matrix. This could qualitatively explain the small changes in Cr intensity observed in different KEMS runs.

In order to confirm the link between Cr activities -between runs- and TCP formation, another series of KEMS measurements could involve measurements with fewer runs of heating and cooling. Metallographic examination would then establish the extent of TCP formation and link this to the determined Cr activities and therefore Cr partial pressures. It is expected that Cr activities behave inversely proportional to the volume fraction of TCP phases within the surface layer.

TCP formation during KEMS measurements is rarely observed and could be explored further as a method to develop deeper understanding of TCP phase formation. TCP phases in Ni-based superalloys are often metastable and the conditions in KEMS could assist studies of TCP formation close to equilibrium.

Similar KEMS studies on the activities of species in alloys have been reported for steels with 3-5 species [65], and others on more complex systems of the Ni-based Inconel 617 and Nimonic PE 13 [66]. A more recent study has looked at the Ni-Al-Cr system [25]. Besides insight into the thermodynamics of single crystal superalloys, the present results are very important for studying the mechanisms of reactions occurring on the surface of such complex systems with the subsequent effect of bulk diffusion, as for example outlined in Ref. [61, 64]. The measured activities are also of great importance for the interpretation of oxidation experiments [13].

The discussion of the findings raises questions that are important beyond the thermodynamic data of the studied alloys. These questions address how KEMS measurements are conducted for alloys of this complexity. Traditionally KEMS measurements hold samples at specific temperature until thermodynamic equilibrium between the sample and the gas phase is established. Elements sublimate at the surface, saturating the cell with vapours and thermodynamic equilibrium is established between the condensed and the vapour phases, where the sublimation rate is equal to the corresponding condensation rate of each species.

At this stage changes to the surface composition of the sample have occurred, especially in the present work where only four out of ten main alloying elements sublimate. This will result in diffusion from the bulk of the sample to the surface, and potentially in the formation of new or dissolution of existing phases. As a result the surface composition will keep changing, which will also change the equilibrium between condensed and vapour phase. This change of the equilibrium happens at a rate controlled by solid state diffusion. Overall a dynamic equilibrium involving vaporisation, solid state diffusion and phase transformation is established. It could also be mentioned that the removal of small amounts of vapour from the Knudsen cell for analysis in the mass spectrometer has an effect on the dynamic equilibrium, but the effect of this can be regarded as negligible due to the massive difference in molar volume between condensed and vapour phase.

All these effects are particularly notable for Cr as on one hand the Cr partial pressure is the highest of all four elements (Ni, Co, Cr, Al), while on the other hand the Cr atomic fraction in the alloys is the lowest of the four studied elements. This means that the relative change in Cr concentration in the alloy due to sublimation is the largest. As Cr is a slow diffusing element, it takes longer for Cr to establish a dynamic equilibrium, which explains the different intensities measured between different KEMS runs. The formation of TCP phases, which can dissolve some Cr, also do play a role in this.

In summary, CMSX-4, CMSX-10K and CMSX-10N were studied using KEMS and results yielded some very useful conclusions both for the particular systems but also for how this

method could be developed further for studying other alloys with similar complexity. These are not commonly studied using KEMS, but they should be studied more as we have seen when comparing the results of present work to studies on binary alloys, that the latter are not necessarily sufficient approximation to multicomponent elemental interactions.

KEMS measurements in multicomponent alloys come with specific challenges. According to Gibbs phase rule equal number of chemical elements and phases have to be present in the condensed phase in order to fix phase compositions, i.e. there have to be three solid phases in a ternary alloy. Changes in alloy composition then result in changes of phase fraction, but phase composition – and therefore activities – remain the same. This approach is commonly used for binary alloys and is certainly feasible for ternary alloys, but it is clearly impractical for the ten component alloys studied in the present work. Different approaches are therefore needed for higher order alloys. This could involve rapid heating of 'virgin' samples to measurement temperature, 'quick' measurement and cooling before significant changes in compositions take place. Traditionally in KEMS, holding at temperature for a long time yield better results. Further work is needed in order to establish if this is equally true for multicomponent alloys, such the ones studied in the present work.

Conclusion

Knudsen Effusion Mass Spectrometry (KEMS) measurements were performed in the γ+γ´ two-phase temperature regions of the second and third generation single crystal superalloys CMSX-4, CMSX-10K, CMSX-10N. Using the KEMS method, the activities of the sublimating elements were determined. The microstructures of samples after KEMS were studied using SEM and EDS.

During KEMS measurements in the temperature range (1453 - 1573) K, the vapour composition of four species: Ni, Co, Cr, and Al were detected. The signal for Cr was decreased after each of the first two runs. Microstructure imaging revealed a reaction surface-layer with TCP's which is related to elemental loss due to sublimation. Results showed the temperature -and composition- dependency of the determined activities.

The thermodynamic behaviour is found as expected: the activities of the four species are depending on their atomic fraction and temperature, except for Al, were an increase in atomic fraction led to a decrease in Al activity. Nevertheless, the present findings depict the complex nature of these alloys and how susceptible they are to microstructural instabilities: i.e. formation of TCP phases.

Experimentally, very few KEMS results are reported in the open literature for this type of alloys. These results are not only very useful in the interpretation of microstructure changes during processing that involve surface reactions, such as oxidation or coating, but also can assist in optimising thermodynamic assessments of this class of alloys. The implications of the multicomponent nature of the alloy on the modus operandi of KEMS are discussed, and suggestions for the development of the method for complex alloys are made.

Acknowledgements

This work was funded via Rolls-Royce plc and Innovative UK as part of SAMULET2 Programme for providing the funding for KEMS experiments to take place in Forschungszentrum Jülich GmbH, Institute of Energy and Climate Research (IEK-2), Jülich, Germany. The authors gratefully acknowledge Dr. Daniel Grüner's and Dr. Egbert Wessel's contribution for providing the back-scattered images and carrying out the compositional analysis of the samples, and Mr Volker Gutzeit's help (Forschungszentrum Jülich GmbH) with carrying out the process of metallography. Also, many thanks to Frank Biddlestone (School of Metallurgy & Materials, University of Birmingham, Birmingham, United Kingdom) for his help with the DSC measurements. Amongst the sponsors, the authors would like to thank the Scholarship Selection Committee of the CALPHAD XLVII Conference and the Armourers & Brasiers Gauntlet Trust.

References

1. Versnyder, F.I. and M.E. Shank, *The development of columnar grain and single crystal high temperature materials through directional solidification.* Mater Sci Eng, 1970. **6**(4): p. 213-247.
2. Sims, T.C., S.N. Stoloff, and C.W. Hagel, *Superalloys II*. 1987, Canada: John Wiley & Sons, Inc.
3. Pollock, T.M. and S. Tin, *Nickel-based superalloys for advanced turbine engines: chemistry, microstructure and properties.* J Propulsion Power, 2006. **22**(2): p. 361-374.
4. Reed, R.C., *The Superalloys: Fundamentals and Applications*. 2006, New York: Cambridge University Press.
5. Ochial, S., Y. Oya, and T. Suzuki, *Alloying behaviour of Ni3Al, Ni3Ga, Ni3Si and Ni3Ge.* Acta Metall, 1984. **32**(2): p. 289-298.
6. Warnken, N., *Studies on the Solidification Path of Single Crystal Superalloys.* J Phase Equilib Diff, 2016. **37**(1): p. 100-107.
7. Giamei, A. and D. Anton, *Rhenium additions to a Ni-base superalloy: effects on microstructure.* Metall Trans A, 1985. **16**(11): p. 1997-2005.
8. Erickson, G., *The development and application of CMSX-10.* Superalloys 1996, 1996: p. 35-44.
9. Broomfield, R.W., et al., *Development and turbine engine performance of three advanced rhenium containing superalloys for single crystal and directionally solidified blades and vanes.* J Eng Gas Turb Pow, 1998. **120**(3): p. 595-608.

10. Pessah, M., P. Caron, and T. Khan, *Effect of mu phase on the mechanical properties of a nickel-base single crystal superalloy.* ONERA, TP, 1992(1992-153): p. 567-576.
11. Reed, R.C., T. Tao, and N. Warnken, *Alloys-By-Design: Application to nickel-based single crystal superalloys.* Acta Mater, 2009. **57**(19): p. 5898-5913.
12. Lukas, H.L., S.G. Fries, and B. Sundman, *Computational thermodynamics : the Calphad method*. 2007, Cambridge ;: Cambridge University Press.
13. Reynolds, T.D., et al., *Identifying heating rate dependent oxidation reactions on a nickel-based superalloy using synchrotron diffraction.* Acta Mater, 2019. **181**: p. 570-583.
14. Belton, G.R. and R.J. Fruehan, *Determination of activities by mass spectrometry. I. The liquid metallic systems iron-nickel and iron-cobalt.* J Phys Chem, 1967. **71**(5): p. 1403-1409.
15. Drowart, J. and P. Goldfinger, *Investigation of inorganic systems at high temperature by mass spectrometry.* Angew Chem Int., 1967. **6**(7): p. 581-596.
16. Grimley, R.T. and J.L. Margrave, *The Characterization of High Temperature Vapors* Mass Spectrometry. 1967, New York: Wiley. 195-243.
17. Neckel, A. and S. Wagner, *Massenspektrometrische Bestimmung thermodynamischer Aktivitäten. I. Das System Gold–Kupfer.* Ber Bunsenges Phys Chem, 1969. **73**(2): p. 210-217.
18. Cater, E.D., *The effusion method at age 69: current state of the art.* Characterization of high temperature vapors and gases, 1979. **1**: p. 3-38.
19. Hilpert, K., *High temperature mass spectrometry in materials research.* Rapid Commun Mass Spectrom, 1991. **5**(4): p. 175-187.
20. Copland, E.H. and N.S. Jacobson, *Measuring thermodynamic properties of metals and alloys with Knudsen effusion mass spectrometry.* 2010.
21. Copland, E.H. and N.S. Jacobson, *Measuring Thermodynamic Properties of Metals and Alloys*, in *Mass Spectrometry Handbook*. 2012, John Wiley & Sons, Inc. p. 1143-1180.
22. Hilpert, K., et al., *Phase diagram studies on the Al-Ni system.* Z Naturforsch, 1987. **42A**(11): p. 1327.
23. Hilpert, K., et al., *Thermodynamic Study of the Liquid and Solid Alloys of the Nickel-Rich Part of the Al-Ni Phase-Diagram Including the AlNi3 Phase.* Ber Bunsen Phys Chem, 1990. **94**(1): p. 40-47.
24. Copland, E., *Formation of gamma '-Ni3Al via the peritectoid reaction: gamma+beta (+Al2O3) = gamma '(+Al2O3)*, in *Superalloys 2008*, R.C. Reed, et al., Editors. 2008, Minerals, Metals & Materials Soc: Warrendale. p. 671-679.
25. Dong, Z.H., et al., *Vaporization of Ni, Al and Cr in Ni-Base Alloys and Its Influence on Surface Defect Formation During Manufacturing of Single-Crystal Components.* Metall Mater Trans A, 2020. **51**(1): p. 309-322.
26. Gibbs, J.W., *ART. LII.--On the Equilibrium of Heterogeneous Substances.* Am J Sci and Arts (1820-1879), 1878. **16**(96): p. 441.
27. Swalin, R.A., *Thermodynamics of solids*. 2nd ed. Wiley series on the science and technology of materials. 1972, New York: Wiley-Interscience. xii,387p.
28. Gaskell, D.R., *Introduction to the Thermodynamics of Materials*. 4th ed. 2009, London, UK: Taylor & Francis.
29. Smith, J.M., H.C. Van Ness, and M.M. Abbott, *Introduction to chemical engineering thermodynamics*. 6th, international ed. McGraw-Hill chemical engineering series. 2001, Boston, Mass.: McGraw-Hill.
30. Hillert, M., *Phase equilibria, phase diagrams and phase transformations: their thermodynamic basis*. 2007: Cambridge University Press.
31. Kobertz, D., C. Guguschev, and M. Müller, *Investigations at High Temperature in Both Equilibrium and Kinetic State with Knudsen Effusion Mass Spectrometry (KEMS) and a Skimmer Integrated Coupling System of Mass Spectrometer and Thermal Analysis (STAMS).* Open Thermodynamics Journal, 2013. **7**(1): p. 71-76.

32. Kobertz, D., M. Müller, and A. Molak, *Vaporization and caloric studies on lead titanate.* Calphad, 2014. **46**(0): p. 62-79.
33. Jacobson, N.S. *Development of the KEMS Technique*. 2012; Available from: https://sites.google.com/site/kemsonline/the-technique, [Assessed: 27.10.2015].
34. Mann, J.B., *Ionization Cross Sections of the Elements Calculated from Mean-Square Radii of Atomic Orbitals.* J Chem Phys, 1967. **46**(5): p. 1646-1651.
35. Deutsch, H., K. Becker, and T.D. Märk, *A modified additivity rule for the calculation of electron impact ionization cross-section of molecules ABn.* Int J Mass Spectrom Ion Processes, 1997. **167–168**: p. 503-517.
36. Deutsch, H., et al., *Extension of the DM formalism for the calculation of cross sections for the multiple ionization of atoms to the formation of highly charged ions.* Int J Mass Spectrom Ion Processes, 1997. **171**(1–3): p. 119-126.
37. Mann, J. *Recent developments in mass spectrometry*. in *Proceedings of the Conference on Mass Spectroscopy, Tokyo, University Park Press, Baltimore, MD*. 1970.
38. Drowart, J., et al., *High-temperature mass spectrometry: Instrumental techniques, ionization cross-sections, pressure measurements, and thermodynamic data (IUPAC Technical Report).* Pure Appl Chem, 2005. **77**(4): p. 683-737.
39. Bell, K.L., et al., *Recommended Data on the Electron Impact Ionization of Light Atoms and Ions.* J of Phys and Chem Ref Data, 1983. **12**(4): p. 891-916.
40. Freund, R.S., et al., *Cross-section measurements for electron-impact ionization of atoms.* Phys Rev A, 1990. **41**(7): p. 3575.
41. Raj, D., et al., *Thermodynamic activity measurements in the B2 phases of the Fe–Al and Ni–Al systems.* Intermetallics, 2003. **11**(11–12): p. 1119-1124.
42. Nakajima, K., *Determination of Optimal Vapor Pressure Data by the Second and Third Law Methods.* Mass Spectrom (Tokyo, Japan), 2016. **5**(2): p. S0055-S0055.
43. Eckert, M., D. Kath, and K. Hilpert, *Thermodynamic activities in the alloys of the Ti-Al-Nb system.* Metall Mater Trans A, 1999. **30**(5): p. 1315-1326.
44. Acharya, M.V. and G.E. Fuchs, *The effect of long-term thermal exposures on the microstructure and properties of CMSX-10 single crystal Ni-base superalloys.* Mat Sci EngA-Struct, 2004. **381**(1–2): p. 143-153.
45. MacLachlan, D.W., et al., *Constitutive modelling of anisotropic creep deformation in single crystal blade alloys SRR99 and CMSX-4.* Int Journal of Plast, 2001. **17**(4): p. 441-467.
46. D'Souza, N.D. and H.B. Dong. *An Analysis of Solidification Path in The Ni-base Superalloy CMSX10K*. in *Superalloys 2008*. 2008. The Minerals, Metals & Materials Society (TMS).
47. Brewster, G., et al., *Surface Segregation during Directional Solidification of Ni-Base Superalloys.* Metall and Mater Trans B, 2008. **39**(1): p. 87-93.
48. Sansonetti, J.E., W. Martin, and S. Young, *Handbook of basic atomic spectroscopic data.* Carbon, 2005. **100**: p. 1634.
49. Burdo, R. and G. Morrison, *Table of atomic and molecular lines for spark source mass spectrometry of complex sample-graphite mixes.* Department of Chemistry, Cornell University, Ithaca, NY, U. SA, 1971.
50. Belov, G.V., V.S. Iorish, and V.S. Yungman, *IVTANTHERMO for Windows — database on thermodynamic properties and related software.* Calphad, 1999. **23**(2): p. 173-180.
51. Bale, C.W., et al., *FactSage thermochemical software and databases, 2010–2016.* Calphad, 2016. **54**: p. 35-53.
52. *OHAUS Analytical Scales and Laboratory Balances*. 2016; Available from: https://www.techadv.com.au/ohaus/, Assessed 15.09.2016].
53. Gurvich, L., et al., *IVTANTHERMO—A Thermodynamic Database and Software System for the Personal Computer.* NIST Special Database, 1993. **5**.

54. Chase, M.W.J., *NIST-JANAF Themochemical Tables*, in *Journal of Physical and Chemical Reference Data*. 1998, National Institute of Standards and Technology Gaithersburg, Maryland. p. 1-1951.
55. Alcock, C., V. Itkin, and M. Horrigan, *Vapour pressure equations for the metallic elements: 298–2500K.* Can Metall Quart, 1984. **23**(3): p. 309-313.
56. Rae, C.M.F., M.S. Hook, and R.C. Reed, *The effect of TCP morphology on the development of aluminide coated superalloys.* Mat Sci Eng-A Struct, 2005. **396**(1–2): p. 231-239.
57. Suzuki, A., et al., *Secondary reaction zones in coated 4th generation Ni-based blade alloys.* Superalloys 2008, 2008: p. 777-786.
58. Suzuki, A. and C.M.F. Rae, *Secondary Reaction Zone Formations in coated Ni-base Single Crystal Superalloys.* J Phys Conf Ser, 2009. **165**: p. 012002.
59. Schneider, C.A., W.S. Rasband, and K.W. Eliceiri, *NIH Image to ImageJ: 25 years of image analysis.* Nat Methods, 2012. **9**(7): p. 671-675.
60. D'Souza, N. and H.B. Dong, *Determination of transition temperatures during freezing and melting of interdendritic phases in Ni based superalloys.* Mater Sci and Technol, 2011. **27**(1): p. 325-331.
61. Wang, H., et al., *Effects of elemental vaporization and condensation during heat treatment of single crystal superalloys.* Scr Mater, 2014. **78**: p. 45-48.
62. Oforka, N., *Thermodynamics of aluminium-nickel alloys.* Indian J Chem, 1986. **25A**: p.1027-1029.
63. Narasimhan, T.S.L., et al., *Activity measurements on the Al-rich region of the Ni–Al system – A high temperature mass spectrometric study.* Z Metallk, 2006. **97**(4): p. 461-470.
64. Spathara, D., D. Putman, and N. Warnken, *Study into the Role of Nickel Vapor on Surface Modification of a Third-Generation Single-Crystal Superalloy.* Metall Mater Trans A, 2018. **49**: p. 4301–4307.
65. Lee, M., *Activity measurement and its use in predicting phase relationships in stainless steels.* J Nucl Mater , 1989. **167**: p. 175-180.
66. Hilpert, K., H. Gerads, and D.F. Lupton, *Mass spectrometric studies of alloys proposed for high temperature reactor systems: II. Inconel alloy 617 and nimonic alloy PE 13.* J Nucl Mater, 1979. **80**(1): p. 126-131.